J. Phys. Chem. A **1999,** *103,* 10093−10117

Femtosecond Real-Time Probing of Reactions. 24. Time, Velocity, and Orientation Mapping of the Dynamics of Dative Bonding in Bimolecular Electron Transfer Reactions[†]

Dongping Zhong, Thorsten M. Bernhardt, and Ahmed H. Zewail*

Arthur Amos Noyes Laboratory of Chemical Physics, California Institute of Technology,
Pasadena, California 91125

Received: June 11, 1999; In Final Form: August 3, 1999

In this paper, we give a full account of our studies of the dynamics of electron-transfer reactions. We examine *bimolecular* reactions of various donors and acceptors and focus on the reversible and dissociative elementary steps probed directly using femtosecond *time*, *speed*, and *angular* resolutions. In particular, we report studies of the bimolecular systems of the following electron donors: diethyl sulfide, *p*-dioxane, acetone, and benzene. The electron acceptors are iodine and iodine monochloride. The general phenomena of reversible and dissociative electron transfer are found for all systems studied. The dynamics of the dative bonding, from the transition state (TS) to final products, involve two elementary processes with different reaction times, speed and angular distributions. For example, for the diethyl sulfide•iodine system, it is shown that after charge separation, the entire complex is trapped in the TS region and the reversible electron transfer occurs in less than 500 femtosecond (lifetime), followed by the rupture of the I−I bond with the release of the first exterior I-atom. However, the second process of the remaining and trapped (caged) interior I-atom takes 1.15 ps with its speed (500 m/s) being much smaller than the first one (1030 m/s). The initial structure is determined to be a nearly linear configuration of S−I−I (165°), consistent with the ab inito calculations and predictions of the HOMO−LUMO frontier orbitals. The observed time scales and bifurcation of the wave packet, with different speeds, are illustrated on the global potential energy surface with the help of molecular dynamics simulations. The findings on this and the other systems reported here elucidate the mechanism and address the concepts of nonconcertedness, caging, and restricted energy dissipation, which are important to the description of reaction mechanisms in the condensed phase, on surfaces, and in electrochemical studies.

I. Introduction

In early theories of chemical bonding by Lewis[1], Pauling[2], Mulliken,[3] and others, the contribution of *covalent* and *ionic* characters is essential to energetics and dynamics and hence to the physical and chemical properties. For many classes of reactions, where the covalent and ionic potential energy surfaces become closer in energy, the description of the dative bond takes into account the two structures, and the wave function becomes:[4]

$$\Psi_{\text{dative}}(D^{+}-A^{-}) = m\Psi_{\text{covalent}}(D-A) + n\Psi_{\text{ionic}}(D^{+},A^{-}) \quad (1)$$

where the covalent and ionic structures are distinct for the “supramolecular” donor (D)−acceptor (A) complex and the coefficients m and n depend on the coupling strength of the two potential energy surfaces (covalent and ionic).

The nature of these charge-transfer (CT) complexes was described by Mulliken in 1952[3] after Hildebrand in 1949 observed a new absorption band in a solution of benzene and iodine dissolved in *n*-heptane.[5] Since then there have been numerous studies in the liquid, gas, and solid phases.[6−9] Ultrafast studies in solutions have revealed the dissociation and caging dynamics on different time scales.[10−13] Under the isolated, binary condition of D and A only recently has the famous benzene-iodine system been studied on the femtosecond[14] and nanosecond[15] time scales. Studies of electron transfer and related processes have provided a microscopic picture in clusters[16] under controlled solvation,[17−19] in a precursor-determined geometry,[20−22] and in matrixes.[23]

For isolated CT reactions between D and A, the dynamics are unique in that the nature of the bond changes with time. With femtosecond time resolution it is possible to prepare the system in a dative ($0 < m < n < 1$) structure by CT excitation and to observe the temporal evolution from the dative-bonding region ($0 < m,n < 1$) to the final ionic ($m = 0$, $n = 1$) or, by reversible electron transfer (RET), covalent ($m = 1$, $n = 0$) structure. In the process, chemical bonds may form or break and the dynamics will elucidate such bond changes following the initial ET. Such processes are relevant in many electrochemical and surface studies.[24−27] The following questions are of central importance to the mechanism: What is the time scale for CT reactions and their possible RET pathways? Are the subsequent chemical events concerted or nonconcerted? What is the geometrical structure in the TS region? And what is the nature of the reaction trajectory, coherent (single-molecule type), or incoherent (ensemble type)?

In this contribution, we give a full account of our studies of this class of reactions. By observing the temporal bond evolutions and the resolution of the speed and angular distributions (see Figure 1A) of the reactions at different times, we are able to elucidate the dynamics and address the above questions. Using femtosecond kinetic-energy resolved time-of-flight (KETOF) mass spectrometry,[28,29] the isolated, bimolecular reactions were studied in a molecular beam. We varied the donors and acceptors to change the initial complex structures and control the energetics, i.e., the location of the CT state.

[†] This article is dedicated to Professor Kent Wilson, the epitome of human decency and passion for science.

10.1021/jp9919359 CCC: $18.00

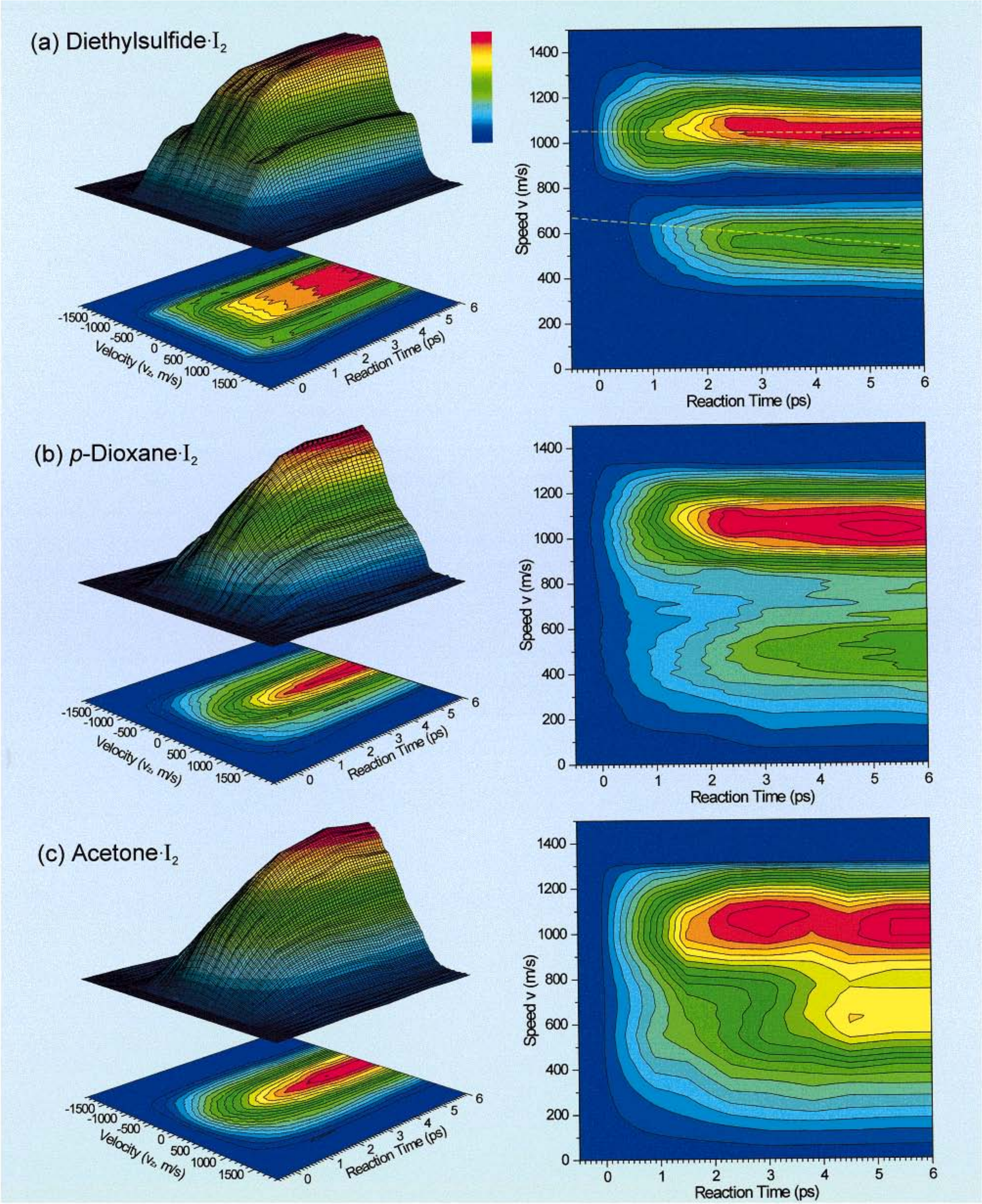

Figure 1 continues

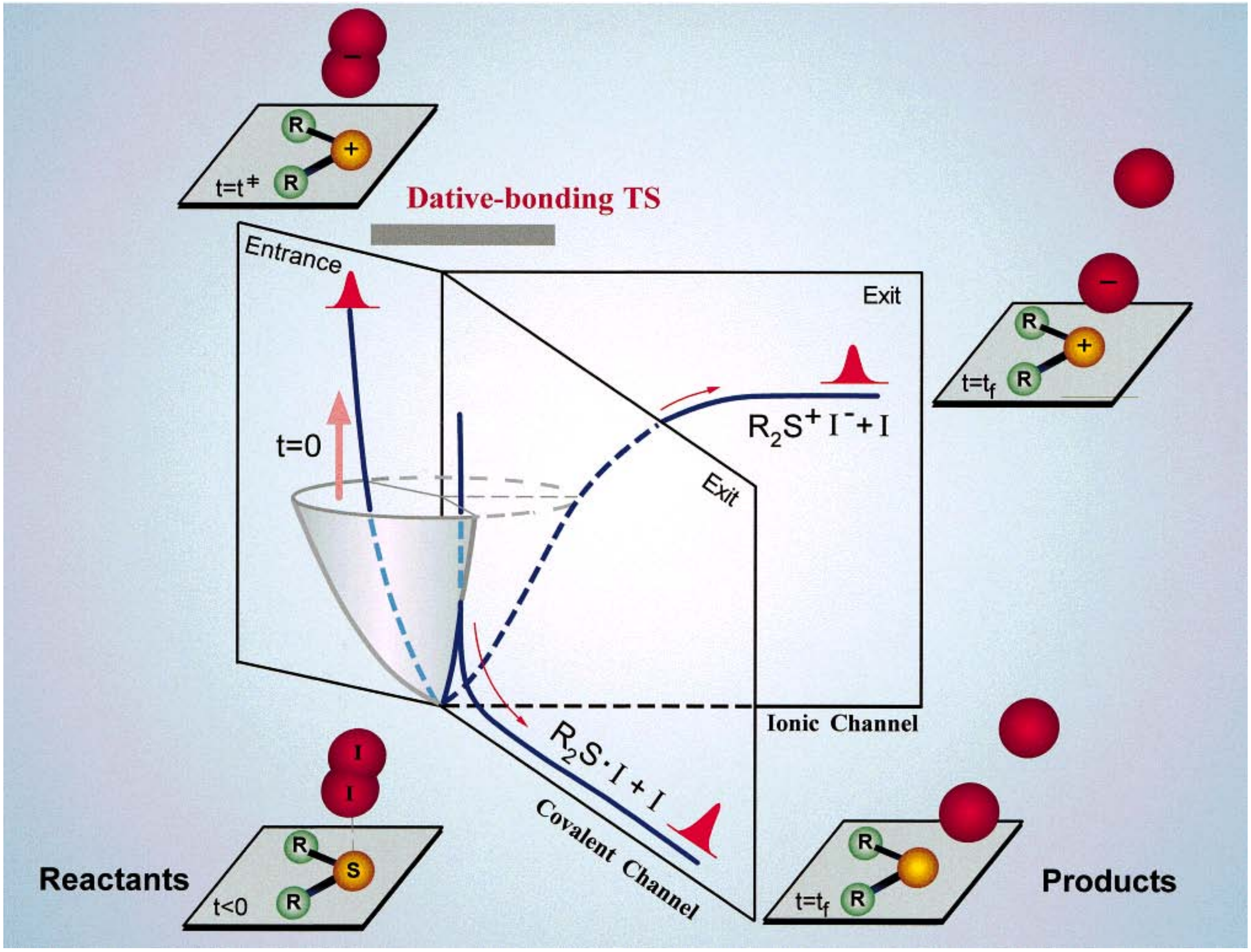

Figure 1 continued

Figure 1. (A, left page) Femtosecond-KETOF resolution of *time*, *velocity (and speed)*, and *orientation* correlations involved in the reaction dynamics reported here: (a) diethyl sulfide•I_2, (b) *p*-dioxane•I_2, (c) acetone•I_2. To the left we display the experimentally observed v_z-time correlations and to the right we display the **v**-time correlations, noting the drastic changes for the different reaction pathways in speed and time. Only one orientation (magic angle) is shown; others are given below. The signal intensity is color coded as represented by the vertical bar on a linear relative scale ranging from 0 (blue) to 100% (red). (B, above) A schematic representation of the multidimensional adiabatic ionic potential energy surface (the elliptic paraboloid) for the bimolecular D•I_2 complex with one cut along the $I^-{-}I$ coordinate for the ionic exit channel. The other cut on the PES results from the crossing with one of the dissociative covalent potential surfaces (the repulsive curve), which leads to a nonadiabatic transition to the covalent exit channel along the I−I coordinate. At zero time, the initial structure is launched at the dative configuration (mostly ionic) by the femtosecond pulse, and the ground-state structure, $R_2S\cdot I_2$ ($R = CH_3CH_2$), is at the vdW distance. The four snapshots show the reaction at $t < 0$, after the electron transfer in the dative-bonding TS region ($t = t^‡$), and after reaching the final ($t = t_f$) products along either the neutral, dissociative covalent or the ionic path. The simplified three-dimensional PES and the corresponding contour maps are depicted in Figures 20 and 21, respectively.

Specifically, we studied diethyl sulfide, *p*-dioxane, acetone, benzene as donors, and iodine and iodine monochloride as acceptors.

In Figure 1B, we present the concept of the experiment, illustrated for the reaction of diethyl sulfide (D) and iodine (A). The femtosecond pulse prepares the complex at $t = 0$, the dative structure, from the structure at the van der Waals (vdW) distance in the neutral ground state. The D•A ground-state bonding is mainly van der Waals in nature while in the CT state it is mostly ionic in character, bound by the Coulomb attraction. The initial excitation induces a femtosecond electron jump from the sulfide donor to the iodine acceptor and suddenly switches on the ionic bonding between the donor and the acceptor. The iodine molecular anion is then rapidly pulled in toward the cation by the strong and attractive Coulomb force, defining the onset for reaction dynamics. For the donor and acceptor themselves, the femtosecond ionization to a localized cation geometry and the vertical electron attachment to a localized anion geometry initiate a nuclear rearrangement in order to achieve the new stable complex structure.

In the transition-state region, which is illustrated in Figure 1B by the elliptic paraboloid, the crossing with one of the dissociative covalent potentials (the repulsive curve) makes possible the evolution toward the covalent character with D•I+I being the products. On the other hand, the reaction pathway may still follow the ionic potential with enough energy flow into the $I-I^-$ bond, leading to D^+I^-+I in the ionic exit channel. However, during the energy redistribution in the TS region, an electron from the acceptor can return back to the donor by a nonadiabatic transition and the dative bond totally transforms into the covalent character, along with the excitation of the donor and/or acceptor. Thus, the time scales of the RET and CT processes determine the critical role of energy dissipation and the relevant nuclear motions important to the structural evolution, the effective dimensionality, and the degree of concertedness.

Experimentally, we follow the dynamics after charge separation by monitoring the evolution of product I-atoms as a function of *time, kinetic energy (speed),* and *orientation.* Similarly, we can follow the decay of the initial complex (the transition state). The kinetic energy resolution of the I-atoms establishes the relative importance of the two pathways, ionic, and covalent. The temporal behavior gives the time scale of the bond evolution, RET, and energy dissipation, and explicates the reaction dynamics. The recoil direction of the exterior I-atom in the complex, relative to the CT transition dipole moment, provides the initial molecular structure. The correlation of the recoil speed and the recoil direction indicates the structural change with the energy release.

The results reported here are striking in demonstrating that, although the initial ET occurs at early times from D to A, an electron from the acceptor reversibly goes back to the donor, leaving the acceptor with enough energy to break the I−I bond. In other words, the initial dative configuration ($0 < m < n < 1$) totally converts to the covalent bonding ($m = 1$, $n = 0$). During this transformation, the dative bond, for instance in the case of diethyl sulfide with I_2, lives for about 500 femtosecond as evidenced by the liberation time of the exterior (i.e., the one away from the donor, the naked one) I-atom. Another striking observation comes from the temporal behavior of the interior (i.e., the one facing the donor, the caged one) I-atom. It is caged *coherently* in the force field of the “substrate” (diethyl sulfide) for 800 femtosecond and completely departs in 1.15 ps. The orientation of the exterior I-atom indicates a nearly linear structure of S−I−I (∼165°, see Figure 1B) in the transition state. These results elucidate the mechanism and provide a clear dynamical picture of the structural changes and the reaction pathways on the time scale of nuclear motions, as detailed below.

This paper is outlined in the following sections, and builds on earlier reports of this class of reactions.[14,30] In section II, we discuss the bonding properties of the complex systems and the CT transition dipole moments. In section III, the experimental techniques are briefly described, including the experimental apparatus and the KETOF method. In section IV, the experimental results are presented. In section V, we discuss the nature of dative bonding and transition states in CT reactions and the caging dynamics. Finally, we give our conclusion in section VI.

II. The CT Systems: Structures, Energetics, and Moments

In what follows, we shall give a brief description of the energetics, transition moments and structures of the systems of interest here.

Beginning in the 1950s, CT complexes have extensively been studied both experimentally[6−9,31−34] and theoretically.[3,4] The experiments focused mainly on the physical and chemical properties of the complex in the ground state, including the binding energy, the equilibrium formation constant, the electronic, vibrational, and NMR spectra, and the complex dipole moments and structures. The observed new UV absorption band from the mixture of the donor and acceptor drew special attentions because it is from neither the donor nor the acceptor molecules alone, and is attributed to the donor−acceptor complex. In Figure 2, a typical example of UV absorption is shown for one of the systems studied here, the diethyl sulfide−I_2 mixture in the gas phase.[35] For an isolated system, the binding energy, structure and electronic spectra are three main properties for characterizing the CT complex.

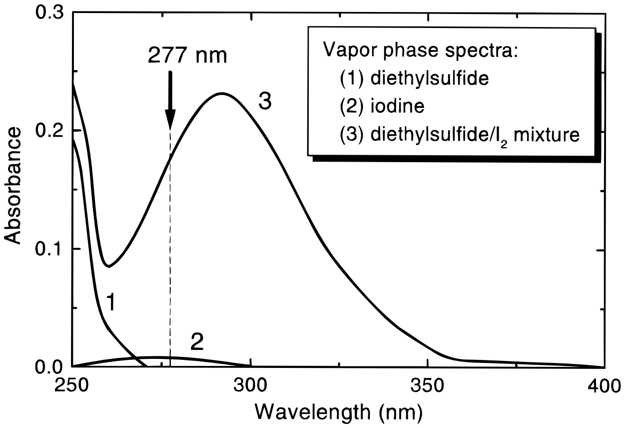

Figure 2. Typical UV absorption spectra of gas-phase diethyl sulfide, iodine, and diethyl sulfide/I_2 mixtures at a temperature of 373 K (adapted from ref 35). Note the large enhancement around 290 nm in the gas mixture. The excitation wavelength (277 nm) used in this work is shown by the arrow.

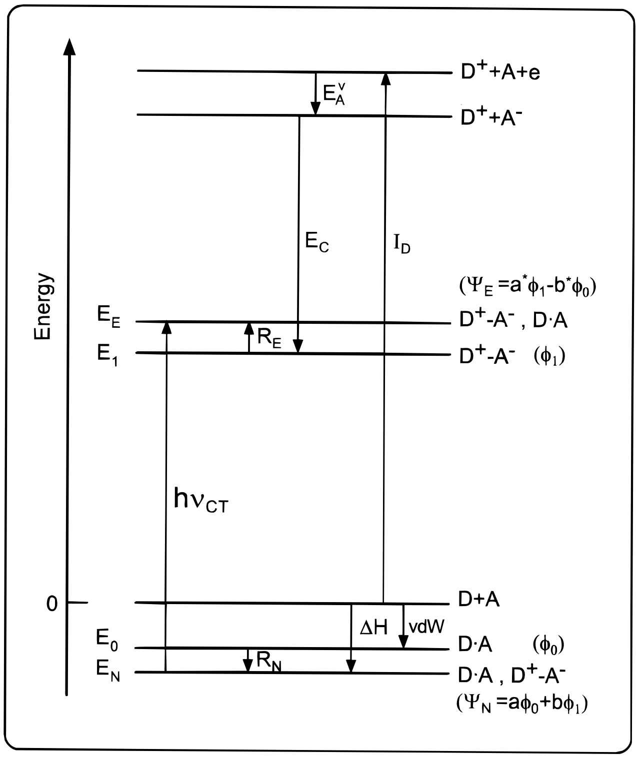

Figure 3. Schematic energy levels of Mulliken’s resonance theory for a donor−acceptor bimolecular complex. R_E and R_N are the *resonance* energies, and E_C is the Coulomb attraction energy. D•A stands for “no-bond” (vdW) configuration and $D^+−A^−$ for the “dative-bond” configuration. Ψ_N and Ψ_E are the wave functions of the ground and CT states, which are mixture of the “no-bond” and “dative-bond” wave functions.

The nature of the bonding in the complex was systematically described by Mulliken.[3,4] The complex is stabilized by resonance interactions between a “no-bond” (D,A) and a “dative-bond” ($D^+−A^−$) ET structures. The energy levels[4,9,34] for a donor−acceptor complex are shown in Figure 3. The ground-state wave function of the complex can, to a first approximation, be written as the sum of two terms

$$\Psi_N = a\phi_0(D,A) + b\phi_1(D^+ - A^-) \tag{2}$$

where ϕ_0(D,A) is the wave function of the no-bond configuration and $\phi_1(D^+−A^−)$ is that of the dative ET configuration. An important requirement for the mixing is that ϕ_0 and ϕ_1 need to be of the same symmetry in the entire D·A complex frame (neglecting vibronic coupling). The no-bond configuration ϕ_0(D,A) mainly results from the vdW interactions, the dispersion force and classic electrostatic multipole interactions between D and A. The dative-bond configuration $\phi_1(\mathrm{D}^+{-}\mathrm{A}^-)$ is conceptually associated with the interaction of molecular orbitals and involves the transfer of an electron from the highest filled donor orbital (HOMO) to the lowest vacant molecular orbital (LUMO) of the acceptor.

The stability and structure of the complexes are very dependent on the particular orbitals that participate in the electron transfer. The donor molecules, according to their HOMOs, can be divided into three types: n, σ, π; the molecule may donate an electron from the n-unshared nonbonding electron pair of a heteroatom (N, O, S), the bonding electron pair of a σ-bond (such as cyclohexane) or from bonding π-electrons (aromatic and unsaturated compounds). The acceptor molecules can also be divided into three types according to the character of the accepting orbitals: υ, σ, π, i.e., the lowest unoccupied molecular orbital (LUMO) is the vacant υ-valence orbital of a metal atom, the antibonding σ-orbital of halogens, or the antibonding π-orbitals (such as tetracyanoethylene, TCNE).

Generally, the interaction of the $\pi\sigma$-complex is relatively weak (∼1−4 kcal/mol),[6,34] and the complex in the ground state is stabilized mainly by the vdW forces. Thus, the no-bond configuration becomes dominant for the weak $\pi\sigma$-complex and the contribution of the dative structure to the ground state is very small. For example, in the benzene·ICl complex, the dative-bond contribution is ≤8.3% ($a \sim 0.93$ and $b \sim 0.28$).[36] The heat of formation is determined to be on the order of −2.54 kcal/mol.[37,38] On the other hand, the nσ-complex usually has a strong binding energy (≥ 3−13 kcal/mol)[6,34] and the dative-bond contribution is not negligible; the dative-bond contribution is 6.5% for p-dioxane·I_2, 12% for diethyl sulfide·I_2 and ∼25% for pyridine·I_2.[9,39] The heat of complex formation is determined to be in the range of −8.3 to −9.0 kcal/mol for diethyl sulfide·I_2 in the gas phase,[35,40,41] −3.3 to −3.8 kcal/mol for p-dioxane·I_2[42,43] in CCl_4, and −3.7 to −5.8 kcal/mol for acetone·I_2 in $C_2F_3Cl_3$.[44−46] The dative-bond contribution changes in the sequence from nitrogen (N)-containing donors (largest), to sulfide (S)- containing donors, and to oxygen (O)-containing donors.

According to Mulliken's theory, the new UV absorption band is simply the excitation of the complex from the ground state to the first CT state and the wave function has the form

$$\Psi_\mathrm{E} = a^*\phi_1(\mathrm{D}^+{-}\mathrm{A}^-) - b^*\phi_0(\mathrm{D,A}) \tag{3}$$

For most CT complexes, the dative-bond configuration is dominant (≥90%) and a^* is much larger than b^*. For example, for the benzene·I_2 complex[9] a^* and b^* are estimated to be in the range of 0.99−0.97 and 0.27−0.36, respectively. Most strong UV absorption bands peak around 250−300 nm (Figure 2), and the excitation energy (Figure 3) can be approximated by the following equality

$$\begin{aligned} h\nu &= \Delta H + I_\mathrm{D} - E_\mathrm{A}^\mathrm{v} - (E_\mathrm{C} - R_\mathrm{E}) \\ &\approx I_\mathrm{D} - E_\mathrm{A}^\mathrm{v} - E_\mathrm{C} \end{aligned} \tag{4}$$

where ΔH is the binding energy of the complex in the ground state, I_D the ionization potential of the donor, E_A^v the vertical electron affinity of the acceptor, E_C the Coulomb energy, and R_E the resonance energy. Usually, the CT excitation energy can be estimated from $I_\mathrm{D} - E_\mathrm{A}^\mathrm{v} - E_\mathrm{C}$ because ΔH and R_E are very small comparing with the other three terms. Spectroscopic studies of a variety of electron donor−acceptor systems have in many cases confirmed this correlation of the CT band energy with the I_D and E_A^v.[4,6−9,31−34] The UV absorption, using I_2 as an electron acceptor ($E_\mathrm{A}^\mathrm{v} \approx 1.0$ eV),[47] peaks at 290 nm[35,40,48] for diethyl sulfide·I_2 ($I_\mathrm{D} = 8.7$ eV), 270 nm[48] for p-dioxane·I_2 ($I_\mathrm{D} = 9.13$ eV) and 242 nm[46] for acetone·I_2 ($I_\mathrm{D} = 9.7$ eV). For the benzene·ICl complex, the CT absorption peak is located at ∼282 nm[49] ($I_\mathrm{D} = 9.24$ eV) but with a larger E_A^v (∼1.5 eV).[50,51]

The electronic transition dipole moment corresponding to the CT excitation is given by

$$\boldsymbol{\mu}_\mathrm{CT} = \langle\Psi_\mathrm{E}|\hat{\mu}|\Psi_\mathrm{N}\rangle = a^*b\boldsymbol{\mu}_{11} - ab^*\boldsymbol{\mu}_{00} + (aa^* - bb^*)\boldsymbol{\mu}_{10} \tag{5}$$

$\boldsymbol{\mu}_{00}$ and $\boldsymbol{\mu}_{11}$ are simply the static dipole moments of the no-bond and dative-bond configurations, and $\boldsymbol{\mu}_{10}$ is the transition dipole moment between them. The $\boldsymbol{\mu}_{11}$ is approximately about eR (R is the distance between the centers of charge of D^+ and A^-) and for typical vdW separations, the magnitude is of the order of 20 D. The direction points from the "center of charge" of D^+ to that of A^-. On the other hand, $\boldsymbol{\mu}_{00}$ is nearly zero or very small (≤ 4 D).[9] For example, the magnitude of the $\boldsymbol{\mu}_{00}$ is about 4.0 D for diethyl sulfide·I_2[52] and 1.0 D for p-dioxane·I_2.[39,53,54] Thus, eq 5 reduces to

$$\boldsymbol{\mu}_\mathrm{CT} \approx a^*b\boldsymbol{\mu}_{11} + aa^*\boldsymbol{\mu}_{10} \tag{6}$$

indicating that the CT transition dipole moment is dominated by two major components. The magnitude of $\boldsymbol{\mu}_{10}$ has been shown by Mulliken[4] to be roughly proportional to the spatial overlap of the donating and accepting orbitals and the direction is determined by the group theory and the CT-state symmetry. Since D and A are in a vdW contact, this component is expected to be small.

For the strong nσ-complex, b is large enough and $\boldsymbol{\mu}_\mathrm{CT}$ is dominated by the $\boldsymbol{\mu}_{11}$ component. Thus, for diethyl sulfide·I_2, p-dioxane·I_2 and acetone·I_2 complexes, the transition dipole moment $\boldsymbol{\mu}_\mathrm{CT}$ points from the heteroatom (S, O) to the center of I_2. For the weak $\pi\sigma$-complexes, it is difficult to judge the relative importance of the two components because of the small mixing coefficient b and it might differ from case to case. However, the $\boldsymbol{\mu}_{10}$ component alone is certainly not enough to explain the observed strong CT transition in the $\pi\sigma$-complex and it turns out in most cases that the $\boldsymbol{\mu}_{11}$ term also makes a major contribution to the CT transition. For the benzene·I_2 and benzene·ICl complexes, the $\boldsymbol{\mu}_{11}$ points from the center of charge of benzene to that of I_2 or ICl, and the $\boldsymbol{\mu}_{10}$ is determined from the point group and the CT-state symmetry, as analyzed in detail in the previous benzene·I_2 studies.[14] Experimentally, by measuring the vector correlation between $\boldsymbol{\mu}_\mathrm{CT}$ and the recoil velocity of the I-atom (v_I) in term of the anisotropy parameter (β), the complex structure is obtained, as shown below.

Figure 4 shows the ab initio structures[55−58] for the different complexes we studied, except for the p-dioxane·I_2 geometry which is taken from the X-ray crystal structure of p-dioxane·I_2.[59] The isolated 1:1 complex geometries predicted from recent ab initio calculations[57,58,60] are found to be very similar to the early X-ray crystal structures,[61] and most geometries can be rationalized by a mutual orientation between D and A to reach a maximum overlap of the donating and accepting orbitals. For the large size of the I-atom, the electrostatic effect also plays

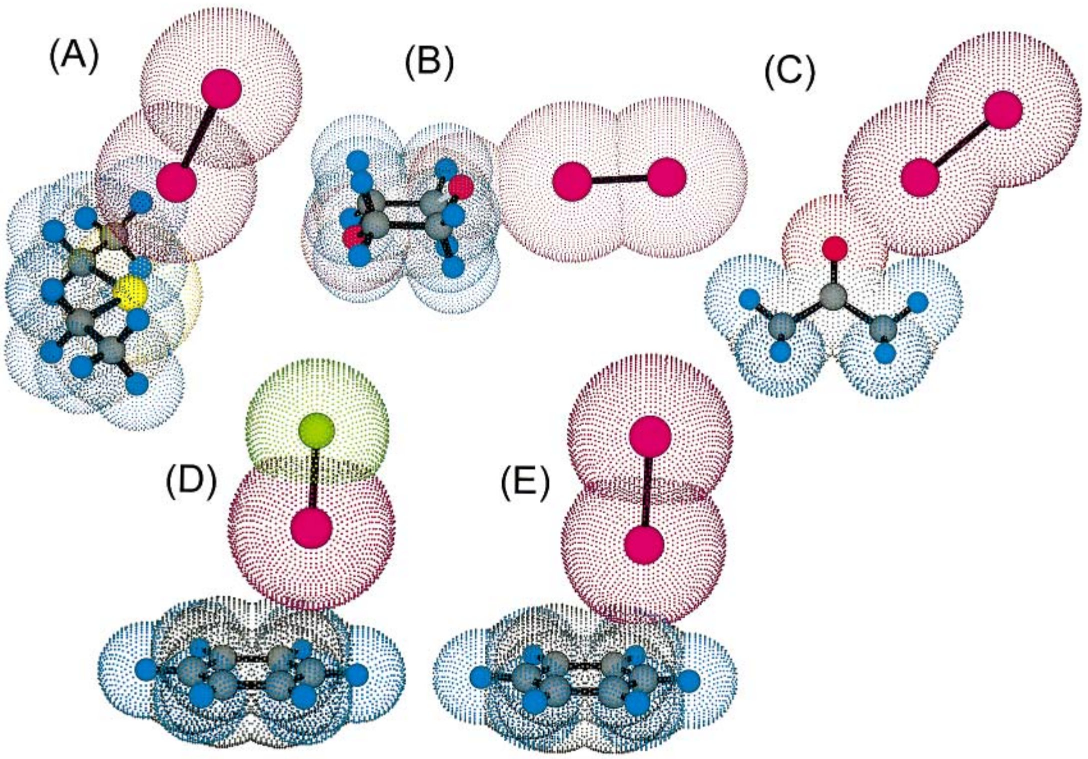

Figure 4. Molecular structures of 1:1 bimolecular, donor−acceptor complexes based on the recent results of ab initio calculations: (A) diethyl sulfide•I_2,[55] $R_{S-I} = 3.3$ Å, $\theta_{S-I-I} = 175°$ and $\theta_{C-S-I} = 97°$; (B) *p*-dioxane•I_2,[59] $R_{O-I} \approx 2.8$ Å, $\theta_{O-I-I} \approx 180°$ and $\theta_{C-O-I} \approx 116°$; (C) actone•$I_2$,[56] $R_{O-I} = 2.8$ Å, $\theta_{O-I-I} = 180°$ (fixed) and $\theta_{C-O-I} = 132°$. Two minimum structures were found for benzene•ICl and benzene•I_2, C-atom centered or C−C bond centered, and only C−C bond centered structures are shown here: (D) benzene•ICl,[57] $R_{C-I} = 3.03$ Å, $\theta_{C-I-Cl} = 177.5°$; (E) benzene•I_2,[58] $R_{C-I} = 3.15$ Å, $\theta_{C-I-I} = 175°$. Note that the structures of D and E are nearly the same.

an important role in forming the ground-state complex. All structures have a C_s symmetry. For the diethyl sulfide•I_2 complex,[55] the calculated binding energy is −6.18 kcal/mol, stabilized by the interaction of the π-type lone-pair electrons ($3p^2$) on sulfur with the I−I σ^* orbital. For the acetone•I_2 complex,[56] the binding energy is calculated to be −5.08 kcal/mol with the sp^2-type lone-pair electrons on oxygen interacting with the σ^* orbital of I−I. The benzene•ICl complex[57] has a binding energy of −3.19 kcal/mol with the I-atom facing the C-atom or the C−C bond center. The ab initio predication of the stabilization energy for the *p*-dioxane•I_2 complex is not available yet, but an estimated value is around −4.0 kcal/mol with interaction of the sp^3-type lone-pair electrons on oxygen with I−I (σ^*), and should be close to the case of the acetone•I_2 complex.

III. Experimental and Methodology

A. Experimental Apparatus. All experiments were performed in a two-chamber molecular-beam apparatus integrated with a tunable femtosecond laser system. Most details have been described in two recent publications,[14,29] and only a brief description is given here.

The femtosecond laser pulses from the oscillator were passed through a home-build four-stage pulsed dye amplifier to reach an energy of 300−400 μJ/pulse and were tuned to be centered at ∼609 nm, typically with ∼3−4 nm full width at half-maximum (fwhm). The 277-nm pump pulse (∼5−10 μJ/pulse) was obtained by focusing 80% of the amplified beam into a D_2O solution to generate a white-light continuum, selecting the wavelength from the continuum, reamplifing through another three-stage pulsed dye amplifier and then frequency-doubling through a 0.5-mm KDP nonlinear crystal. The remaining 20% of the 609-nm laser beam were sent to a double-passed single-stage dye amplifier and then delayed in time by a retroreflector mounted on a computer-controlled translation stage. A 0.5-mm KDP crystal was used for frequency doubling to obtain the probe beam at around 304.5 nm (∼20 μJ/pulse) for 2+1 resonance-enhanced multiphoton ionization (REMPI) detection of free iodine atoms. Finally, the pump and probe pulses were recombined collinearly, focused and spatially overlapped in the extraction field region of the TOF mass spectrometer.

A supersonic molecular beam containing the species of interest was generated in the first chamber, skimmed and intersected by the femtosecond laser beams in the extraction region of a two-stage linear TOF-MS housed in the second chamber. The molecular beam, TOF-MS axis, and the femtosecond laser beams were orthogonal to one another. For all results reported here, the pump laser polarization was orthogonal to the probe laser one and either parallel or at an angle of 54.7° to the TOF-MS axis (z). The TOF-MS was also used as a kinetic-energy spectrometer, as described in section III.C, to resolve the speed and angular distributions of reaction products. The pump−probe cross correlation was typically 400 ± 50 femtosecond fwhm. Although a much shorter probe pulse can be easily reached, the resulting broader spectrum leads to the loss of tunability for the iodine-atom REMPI detection. All transients reported here result from one-photon excitation as checked by the pump power dependence of the observed signal.

Molecules of interest were seeded in ∼800 Torr of He and were expanded through the pulsed valve. The mixture was made by flowing the He over the donors and acceptors separately far away from the nozzle and then combining the two gas lines together before the nozzle. To avoid larger cluster formation, except the 1:1 D•A binary complex, the condition was carefully

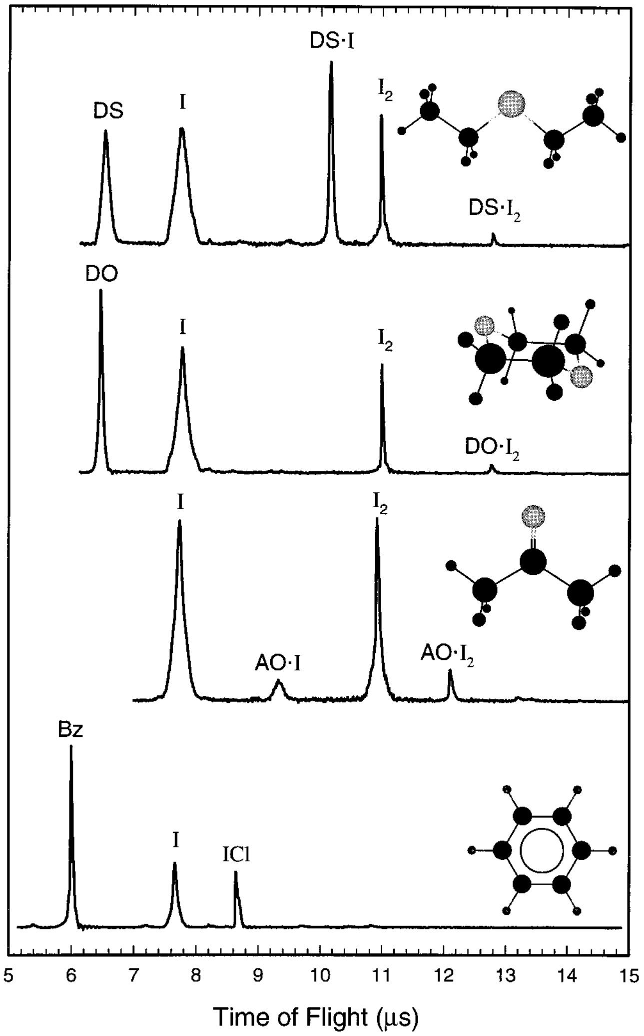

Figure 5. TOF mass spectra under the 1:1 donor−acceptor complex conditions. Careful control was made of the delay time between the femtosecond laser pulses and the pulse valve opening, and the sample temperature. Note that no larger cluster traces except the 1:1 binary complexes were found. The fragmentation is clear. The donor structures are also shown on the right side. DS stands for diethyl sulfide, DO for *p*-dioxane, AO for acetone, and Bz for benzene.

controlled in two ways: sampling the different portion of the gas pulse by varying the delay time between the femtosecond laser pulses and the pulsed valve opening, and keeping the low vapor pressure of the samples by maintaining them at low temperatures.

All samples were purchased from Aldrich. For donors, the diethyl sulfide (DS, ≥ 98% pure), *p*-dioxane (DO, ≥ 99%), acetone (AO, ≥ 99.5%) and benzene (Bz, ≥99.9%) were cooled to −54 °C, −20 °C, −68 °C and −45 °C, providing 0.45 Torr, 2.8, 0.6, and 0.5 Torr of vapors, respectively. For acceptors, the iodine (I_2, 99.999%) was used at room temperature (vapor pressure ~1 Torr). The iodine monochloride (ICl) was sublimated from the iodine trichloride (ICl_3) crystal in order to eliminate the contamination because the vapor above the ICl crystal contains I_2.[62] The existence of excess Cl_2 vapor above the ICl_3 crystal suppresses the I_2 formation due to the reaction of Cl_2 and I_2. The crystalline ICl_3 (≥ 97%) was cooled to −12 °C, giving an estimated ICl vapor of ~2−3 Torr.[62]

B. Mass Spectra. The TOF mass spectra are shown in Figure 5. Note that only the 1:1 donor−acceptor binary complex was formed under the well-controlled conditions and the D·A complex ion fragmentation is evident for most cases, as seen from the small D·A complex TOF signal and broad distributions of fragment mass peaks. Especially for the benzene·ICl, the 1:1 complex ion nearly goes to complete fragmentation. Experimentally, when the donors were added into the I_2/He mixture, the I-atom *transient* intensities were enhanced by a factor of ~14, 4, 5 for diethyl sulfide, *p*-dioxane, and acetone, respectively. For the reaction of benzene with ICl, the I-atom *transient* signal was enhanced by a factor of ~7. The observed enhancement indicates a direct CT excitation and excludes the contributions from the locally excited D*·A and D·A* reactions, in accord with the much stronger absorption of the D·A complex than those of donors[35,46,49,63−65] and acceptors[66,67] alone, as illustrated in Figure 2 for the case of the diethyl sulfide/I_2 mixture.

The fragment mass peak D·I resulting from the 1:1 complex (D·I_2) ion fragmentation, reflects the nature of the bonding between D and I_2/I. As mentioned in section II, the binding energies for diethyl sulfide·I_2, acetone·I_2, *p*-dioxane·I_2 and benzene·ICl are −6.2, −5.1, ~−4.0, and −3.2 kcal/mol, respectively. In Figure 5, the D·I peak is very large for diethyl sulfide·I_2 (DS·I), small for acetone·I_2 (AO·I) and hardly seen for *p*-dioxane·I_2 and benzene·ICl. This is consistent with the D·I_2 (D·I) complex binding energies being relatively large. An attempt was made to study the much stronger complex reactions of pyridine·I_2 and diethyl sulfide·ICl, but it did not work out because some chemical reactions between the donor and the acceptor occur in the mixing line before expansion.

C. Femtosecond-Resolved Speed and Angular Resolutions. To dissect the different elementary processes and elucidate the mechanism involved in the CT reactions, we have used the REMPI detection in combination with femtosecond techniques and a KETOF mass spectrometry to measure the translational energy and angular distributions of the reaction as a function of time. In the following, we will briefly describe the basic ideas of this method.

The translation energy release due to the bond breakage causes a spread in the KETOF profile around the central time T_0 (in TOFMS). Because the time spread ($\Delta T = T - T_0$) is a linear function of the three-dimension velocity projection onto the TOF axis (z), the KETOF profile can be transformed into the velocity ($\mathbf{v}_z$) distribution by the equation

$$\mathbf{v}_z = \Delta T q E/m \tag{7}$$

where m and q are the mass and charge of the ionized fragment I and E is the electric field strength for extraction. In practice, we calibrate for the precise (not apparent) value of E by measuring the known velocity profile of methyl iodine dissociation.[14,29]

As detailed in a recent publication,[29] the observed $\mathbf{v}_z$ distribution, $f(\mathbf{v}_z)$, is sensitive to three parameters, speed distribution $f(\mathbf{v})$, anisotropy β, and angle χ (the pump laser polarization $\hat{\epsilon}_{pu}$ relative to the z axis), by the following equation

$$f(\mathbf{v}_z,\chi) = \int_{|\mathbf{v}_z|}^{\infty} \frac{1}{2\mathbf{v}}\left[1 + \beta(\mathbf{v})P_2(\cos\chi)P_2\left(\frac{\mathbf{v}_z}{\mathbf{v}}\right)\right] f(\mathbf{v})\mathbf{v}^2 d\mathbf{v} \tag{8}$$

where P_2 is the second Legendre polynomial. The speed distribution $f(\mathbf{v})$ is determined by the nature of the bond rupture and the anisotropy β is determined, *on the femtosecond time scale where no rotation needs to be considered*, by the direction θ of the recoil velocity relative to the initial alignment (transition dipole); $\beta = 2P_2(\cos\theta)$. The value of β becomes 2 for a purely parallel ($\theta = 0°$) transition, while for a perpendicular transition ($\theta = 90°$) it is equal to −1.

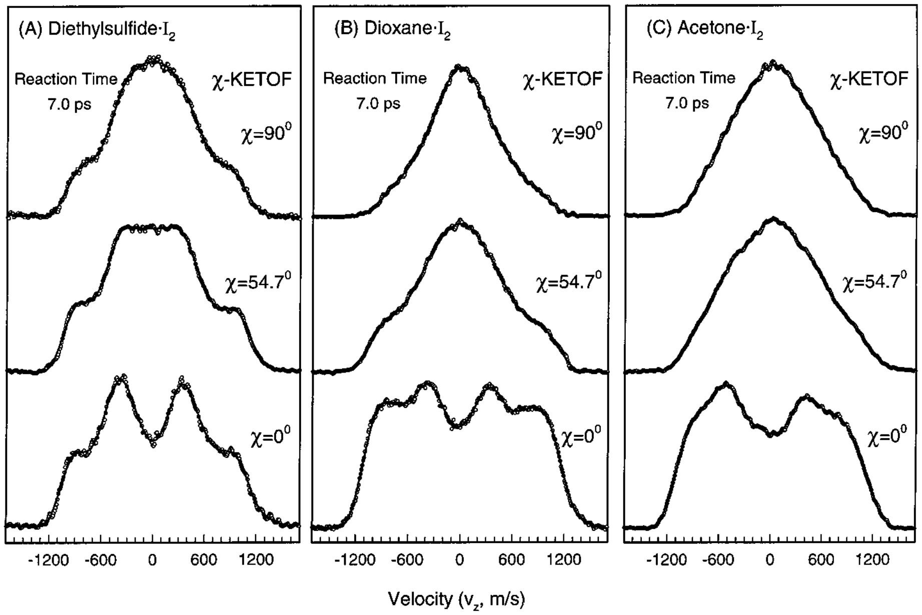

Figure 6. Angular-resolved KETOF distributions for the three different χ's, as indicated, at a fixed delay time of 7.0 ps. All three complexes show a parallel-transition behavior at 277 nm excitation. Note that for each case two velocity distributions are present. The open circles are the experimental data and the smoothed solid lines are shown only for guidance of the eye.

Of particular importance is the special case of $\chi = 54.7°$, or the "magic angle", where $P_2(\cos\chi) = 0$. The distribution is independent of β and becomes

$$f(\mathrm{v}_z, 54.7^0) = \int_{|\mathrm{v}_z|}^{\infty} \frac{1}{2\mathrm{v}} f(\mathrm{v})\mathrm{v}^2 \mathrm{dv} \qquad (9)$$

At this pump angle, the $\mathbf{v}_z$ profile depends only on the scalar speed distribution. Equation 9 allows the speed distribution to be extracted directly by differentiation

$$f(\mathbf{v}) = -\frac{2}{\mathbf{v}} \frac{\mathrm{d}}{\mathrm{d}\mathbf{v}_z} f(\mathbf{v}_z, 54.7^0)|\mathbf{v}_z = \mathbf{v} \qquad (10)$$

The speed probability distribution and the fragment translational energy distribution can be obtained

$$g(\mathbf{v}) = f(\mathbf{v})\mathbf{v}^2, \quad P(E_T) = \frac{g(\mathbf{v})}{m\mathbf{v}} \qquad (11)$$

Once $f(\mathbf{v})$ is known, the anisotropy parameter $\beta(\mathbf{v})$ can also be derived by fitting the $\mathbf{v}_z$ distribution measured at the parallel polarization ($\chi = 0°$) according to eq 8.

Typically, we resolve the I-atom KETOF profiles at $\chi = 54.7°$ for the different delay times (femtosecond-KETOF) to directly obtain the evolution of the speed distributions. We then observe the flux of I-atoms for different pump polarizations at fixed delay times (χ-KETOF) to obtain the evolution of the angular distributions (β). *Using this powerful method, we can obtain femtosecond-resolved speed and angular time evolution of products.* It should be noted that there are two modes of detection, that involving the projection of all velocities and the other is a core-sampling mode using an aperture. Here, we use the former, carefully considering the relative transverse and longitudinal velocities involved.[14,29]

IV. Results

A. Time and Velocity Correlations. The angular-resolved I-atom KETOF distributions (χ-KETOF) for three different pump polarizations are shown in Figure 6 for the three nσ-complexes at a fixed delay time of 7.0 ps. The data were taken very carefully: (1) the pump and probe intensities were kept as low as possible to reduce the space-charge effect and minimize the KETOF broadening, and (2) the I-atom transient KETOF distributions from the background I_2 dissociation in the molecular beam, which accounts for 7% of the total signal for diethyl sulfide•I_2, 25% for *p*-dioxane•I_2 and 20% for acetone•I_2, were subtracted out from each measurement. The iodine molecule was found to have a pure perpendicular transition at 277 nm (C←X)[68] and the KETOF shape[69-72] ($\beta \sim -1.0$) is totally different from those shown in Figure 6, especially at $\chi = 0°$. No noticeable change was found for all KETOF distributions (Figure 6) after 7 ps delay time. These distributions ($\chi = 0°$) clearly indicate that two distinct velocity components are present, especially evident for the diethyl sulfide•I_2 complex. All three systems show a parallel transition and their different shapes reflect the different translational energy and anisotropy distributions of the I-atom release.

To reveal the dynamic behavior of the two velocity distributions, the temporal evolution of the KETOF distributions was measured and for each measurement, the background I-atom transient KETOF distribution was subtracted out. Figure 7 shows the femtosecond-resolved KETOF distributions at the parallel ($\chi = 0°$) and magic angle ($\chi = 54.7°$) polarizations for the diethyl sulfide•I_2 complex. Clearly, two distinct velocity distributions, fast and slow, show a dramatic difference in the temporal behavior. At early times, only the fast I-atoms appear and the distribution reaches a plateau value after 1.75 ps. However, the slow ones show up only after ~900 femtosecond and gradually buildup until 7 ps, and also have a higher anisotropy than the fast ones, as clearly seen from the growth of the two components at $\chi = 0°$.

The femtosecond-resolved KETOF distributions for the *p*-dioxane•I_2 and acetone•I_2 complexes are shown in Figure 8 for $\chi = 54.7°$. Once again, two velocity distributions, fast and slow, are present and have different time behavior. For *p*-dioxane•I_2, the fast I-atoms are released quickly and after 2.26 ps, the signal ($\mathbf{v}_z \geq 800$ m/s) stays constant but the slow distribution keeps growing until 7 ps. For acetone•I_2, although

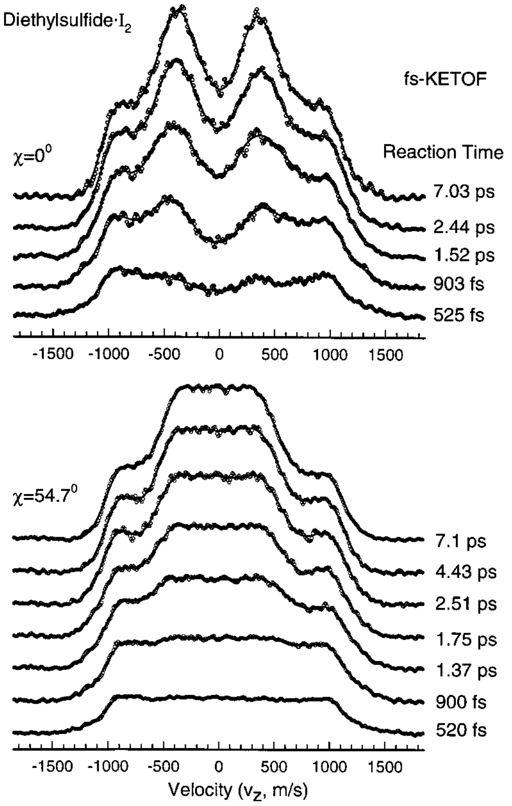

Figure 7. Femtosecond-resolved KETOF distributions at two different χ's ($\chi = 0°$ and 54.7°) for diethyl sulfide•I$_2$. Note the different temporal behavior for the two velocity distributions. The open circles are the experimental data and the smoothed solid lines are shown for guidance of the eye.

the two distributions overlap heavily, the fast distribution at $\mathbf{v}_z \geq 800$ m/s under careful examination shows a constancy after 3.03 ps and the slow I-atom signal continues to increase up to 7 ps.

In Figure 9, the two velocity distributions are clearly revealed in the speed distributions, derived from the magic-angle ($\chi = 54.7°$) data (Figures 7 and 8, Figure 1A). The corresponding translational energy distributions of I-atoms are shown in Figure 10. The high-speed ($\mathbf{v} \geq 800$ m/s) components of the three complexes are very similar whereas the three slow-speed distributions are very different. For diethyl sulfide•I$_2$, the two speed distributions are well separated at v = 800 m/s ($E_T = 3420$ cm^{-1}). For the oxygen-containing donors, the two distributions overlap in the range of 750−850 m/s ($E_T = 3000{-}3860$ cm^{-1}). The dramatic difference in the temporal behavior for the two speed distributions observed here for all three complexes clearly shows that the two types of I-atoms are *from two different dynamic processes of the reaction, not resulting from the parallel reaction pathways involving the two spin−orbit states of I and I** (separated by 7600 cm^{-1}), e.g., for the covalent channel I/I*+D•I/D•I*. Analyses of the two translational energy distributions, as discussed below, also support this conclusion.

The high-speed component is centered at ~1030 m/s (5700 cm^{-1}) and extends to ~1300 m/s (10000 cm^{-1}) for all three complexes. This fast component *is unambiguously assigned to the exterior I-atom released through the dissociative covalent channel*, simply because of energetics. For example, the maximum CT absorption of the diethyl sulfide•I$_2$ complex in the gas phase is at 290 nm[35,40,48] (Figure 2) and recent ab initio calculations[55] give an equilibrium distance of 3.32 Å between S and I, and a binding energy of −6.2 kcal/mol. For a complete ET, the DS$^+$I$^-$ equilibrium distance is derived to be 3.7 Å.[14]

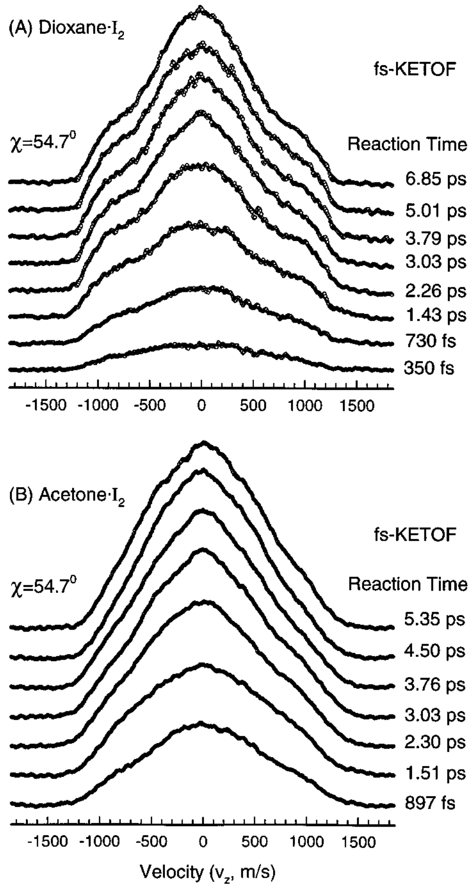

Figure 8. Fs-resolved KETOF distributions at $\chi = 54.7°$ for (A) *p*-dioxane•I$_2$ and (B) acetone•I$_2$. Note the different time evolution of the two velocity distributions. The open circles are the experimental data and the smoothed solid lines are shown only for guidance of the eye.

To account for a fraction ET, we take the value in the range of 2.7−3.7 Å, predicting that the lower limit of the zero-point energy of DS$^+$I$^-$ is ~2.1 eV above its ground state. Therefore, the upper limit of the available energy for the ionic exit channel is ~0.6 eV at 277 nm excitation and the maximum translational energy of the released exterior I-atoms, based on the kinematics, is ~3000 cm^{-1}, much smaller than our observed 10000 cm^{-1} for the fast I-atom. Similar considerations are applied to the other two oxygen-containing complexes. Thus, the presence of such covalent channel indicates that RET must occur and is responsible for the high-speed distribution acquired by the fragment I-atom, much higher than that from the ionic exit channel (see Figure 1B).

For the diethyl sulfide•I$_2$ complex, the slow distribution is centered at a final speed of $v = 500$ m/s (1335 cm^{-1}) but terminates at 300 m/s (480 cm^{-1}). Furthermore, *the peak shifts* (Figure 9A, see also Figure 1A) from the maximum of $\mathbf{v} = 620$ m/s at early times to $v = 500$ m/s after 7 ps, indicating the degree of inelastic energy transfer from the atomic motion to the donor molecule. The slow I-atom release is also from the dissociative covalent channel and any contribution from the ionic one must be negligible. This is supported by the following *five* observations, detailed below: (1) the branching ratio of the fast I-atoms to slow ones, (2) the difference in coherent caging time from the fast I-atom distribution, (3) the difference in anisotropy of the two I-atoms (1−3 as detailed below), (4) the shift of the entire distribution with time (shown above), and (5) the fact that the I-atom distribution observed here did not extend to zero speed, typically observed in many harpoon reactions.[73,74]

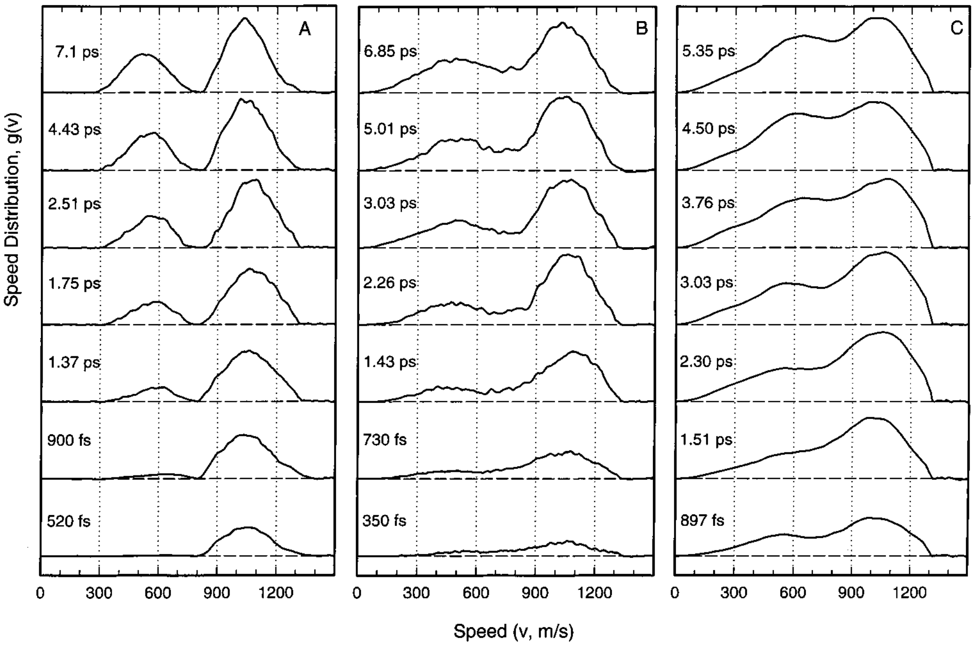

Figure 9. Fs-resolved speed distributions of the I-atoms obtained from $\chi = 54.7°$ magic-angle data of Figs.7 and 8 for (A) diethyl sulfide•I_2, (B) *p*-dioxane•I_2, and (C) acetone•I_2. The two speed distributions are clearly revealed and the slow component shows a dramatic difference in the temporal behavior when compared with the fast one. Note the shift of the slow component with time and the lack thereof in the fast component. In (A), the slow speed distribution terminates at **v** = 300 m/s. A contour map of the speed-time correlations is presented on the right side in Figure 1A.

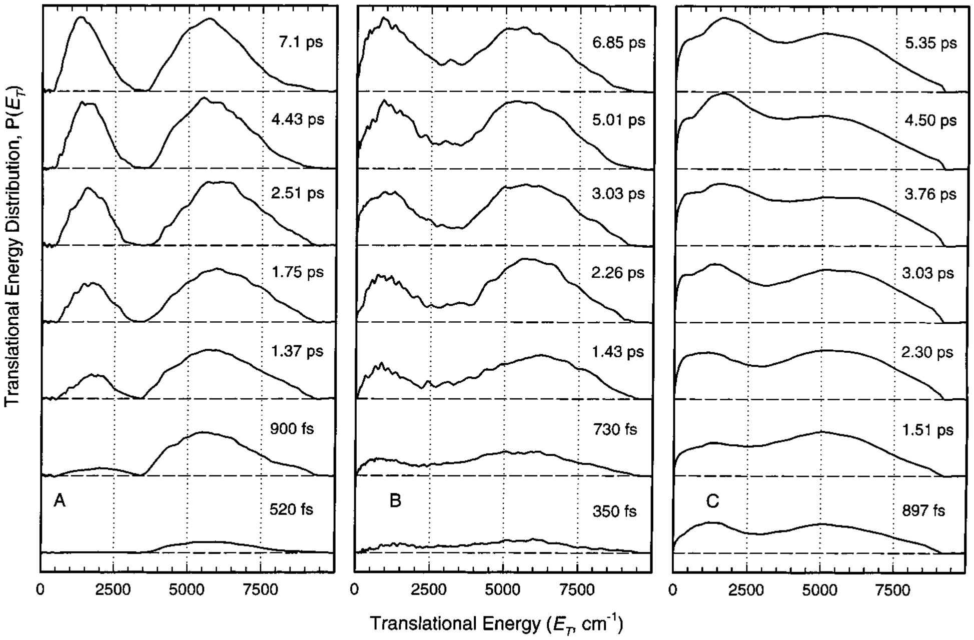

Figure 10. The corresponding translational energy distributions of the I-atoms obtained from the speed distributions (Figure 9) for (A) diethyl sulfide•I_2, (B) *p*-dioxane•I_2, and (C) acetone•I_2. Note that the two distributions are well separated at $E_T \approx 3500$ cm^{-1} for (A) but the two are heavily overlapped for (C).

Accordingly, this slow component results from the interior I-atoms, released from the dissociative covalent channel after collisions with diethyl sulfide in a *one-molecule caging*. Note that the reversible ET ensures the covalent dynamics for both I-atoms, and the above observations suggest that the fraction of the harpoon to the covalent channel is negligible.

For the oxygen-containing donor complexes, although the slow distribution is not well separated from the fast one, similar processes of the one-molecule caging for the slow I-atoms were observed. The slow distribution for *p*-dioxane•I_2 is centered at the final speed of 500 m/s, similar to the diethyl sulfide•I_2 complex, and also changes with time: at the early delay time it terminates at ~200 m/s and at the later delay time (7 ps) extends to 0. The slow component for acetone•I_2 peaks at the final speed of ~600 m/s (1925 cm^{-1}) and gradually extends to 0 with time. Although the contribution from the ionic exit channel for the two oxygen-containing donor complexes could not be exclusively ruled out, it should be negligible based on the following measurements of the branching ratios of the slow I-atoms to the fast ones and the difference in anisotropy for the fast and slow components.

B. Femtosecond Transients and Branching Ratios. The temporal behavior of the two dynamical processes is also revealed clearly by gating of the fast and slow components

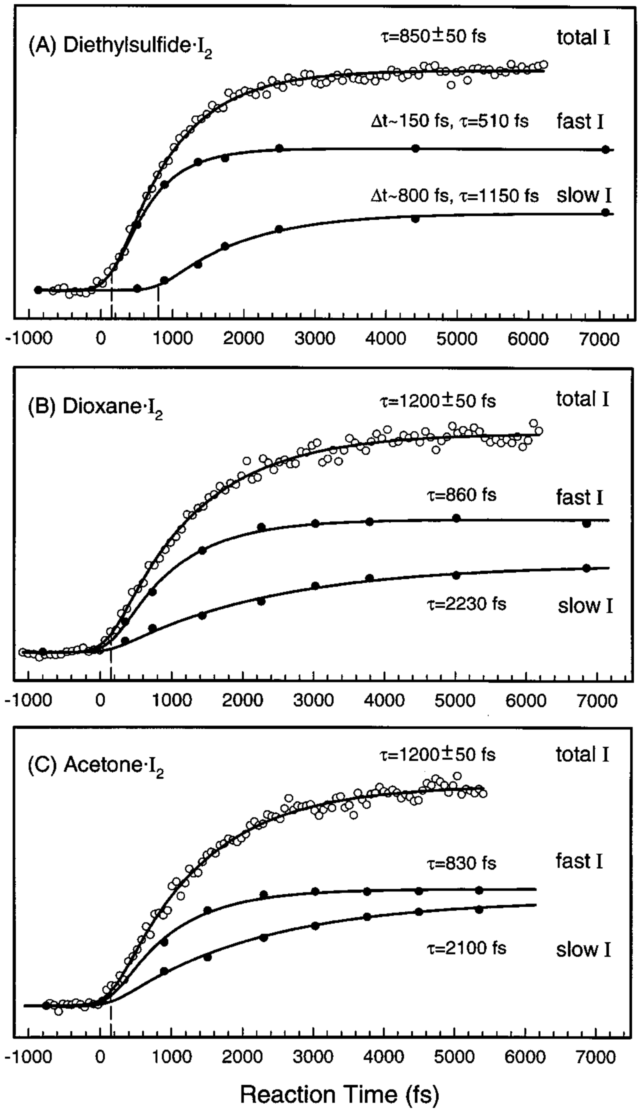

Figure 11. Fs-gating of different speed distributions. Shown are the total iodine atom transients (open circle) and the gated transients (solid circle) of the fast and slow components: (A) diethyl sulfide$\cdot I_2$, (B) *p*-dioxane$\cdot I_2$, and (C) acetone$\cdot I_2$. The branching ratios of the slow to the fast are 55:100, 65:100 and 88:100 for (A), (B), and (C), respectively. The solid lines are the theoretical results fitted using a coherent delay and an exponential rise describing the time evolution (see text). Note that the slow I-atom component of (A) has an 800 femtosecond coherent delay and that all other femtosecond transients show a 150 femtosecond coherent shift.

(using $\mathbf{v} = 800$ m/s as the dividing line of the two distributions for the oxygen-containing complexes). The transients are shown in Figure 11, together with the experimental transients while collecting all I-atoms (the background I-atom transient from the I_2 monomer has been subtracted out). The slow I-atoms show a dramatic difference in time evolution from the fast ones for all cases studied here.

The total I-atom transients give time constants of $\tau = 850$, 1200, and 1200 (± 50) femtosecond for the overall reactions of diethyl sulfide$\cdot I_2$, *p*-dioxane$\cdot I_2$, and acetone$\cdot I_2$, respectively. The fast components, however, give rises of 510, 860, and 830 femtosecond, all with a ~150 femtosecond coherent delay from the time zero, whereas the slow components show rise times of 1.15, 2.23, and 2.1 ps, but with a ~800 femtosecond coherent shift for diethyl sulfide$\cdot I_2$ and only a ~150 femtosecond coherent delay, similar to the fast I-atom transients, for both oxygen-containing complexes.

The reaction time of the exterior I-atom (fast component) represents the I−I bond rupture in the $D\cdot I_2$ system, i.e., the dative-bonding TS lifetime of $D^+{-}^-I{\cdot\cdot}I^\ddagger$. Specifically, the observed 510, 860 and 830 femtosecond reaction times are the entire complex lifetimes of $DS^+{-}^-I{\cdot\cdot}I^\ddagger$, $DO^+{-}^-I{\cdot\cdot}I^\ddagger$ and $AO^+{-}^-I{\cdot\cdot}I^\ddagger$, respectively. Since RET is responsible for the extinction of the dative bonding and the birth of the covalent bonding, *the observed complex lifetime here is actually the time of the overall RET process, of the dative bonding of the complex in the transition state, and of the dissociative covalent bonding formation.* The coherent shift of 150 femtosecond observed for all three complexes indicates the nature of the coherent reaction trajectories and is the shortest time for some trajectories moving from the initial *well-localized* configuration to the final products. This coherent delay equals to the typical I−I bond breaking time on a repulsive potential surface.[29] Thus, after the dative wave packet preparation at $t = 0$, some trajectories quickly hop to the dissociative covalent exit channel by RET and the dative bonding promptly switches to the covalent bonding.

The reaction times of the interior I-atoms (slow component) represent the entire dynamical processes of the CT reactions including the one-molecule caging of the $D{\cdot\cdot}I$ complexes. Specifically, the observed 1.15, 2.23, and 2.1 ps contain the entire complex evolution time and the collision complex lifetimes of $DS{\cdot\cdot}I$, $DO{\cdot\cdot}I$, and $AO{\cdot\cdot}I$, respectively. The observed large coherent shift (800 femtosecond) from $DS{\cdot\cdot}I$ indicates that the interior I-atom was *trapped* in the force field of the donor (DS) during the collision. The 150 femtosecond coherent delay for both $DO{\cdot\cdot}I$ and $AO{\cdot\cdot}I$ gives the shortest time for the interior I-atom to liberate from the force field of both the donor and the fast exterior I-atom. This time equals to the observed coherent shift of the fast exterior I-atom, implying that some trajectories coherently evolve along the three-body pathway to D+I+I after RET.

Since the exterior I-atoms are released from the covalent channel, the interior I-atoms, facing the donor, proceed to an inelastic collision with the donor. For an ideal case in which the interaction between the I-atom and the donor is very weak, the interior I-atoms should be completely liberated and the branching ratio of the slow I-atoms to fast ones is 1. Experimentally, we obtained the branching ratios (after 7 ps in Figure 11) of 55:100 for diethyl sulfide$\cdot I_2$, 65:100 for *p*-dioxane, and 88:100 for acetone$\cdot I_2$. These ratios are all less than 1, indicating that the slow exterior I-atoms from the ionic exit channel are negligible (otherwise, the branching ratio should be larger than 1).

As much as 45% of the caged interior I-atoms are not liberated from the collision complex of $DS{\cdot\cdot}I$, consistent with the strong binding energy, ~ -6 kcal/mol, between diethyl sulfide and the I-atom.[75] Further evidence of the speed cutoff at 300 m/s (Figure 9) for the interior I-atoms indicates that some interior I-atoms with the low translational energy are trapped in the force field of diethyl sulfide and that there exists a barrier for dissociation to DS+I. It is surprising that as much as 35% of the caged I-atoms are trapped in the $DO{\cdot\cdot}I$ collision complex even though the binding energy is not so strong, only −4 kcal/mol. For the $AO{\cdot\cdot}I$ collision complex, only 12% of the interior I-atoms are trapped though the binding energy (−5.1 kcal/mol) is larger than that of the $DO{\cdot\cdot}I$ complex.

C. Recoil Anisotropy and Initial Complex Structure. Because the dynamics of CT reactions occur on the femtosecond time scale, the rotational motion is negligible, and, therefore, the measured recoil anisotropy of I-atoms reflects the vectorial correlation (θ, $\beta = 2P_2(\cos\theta)$) between the recoil direction

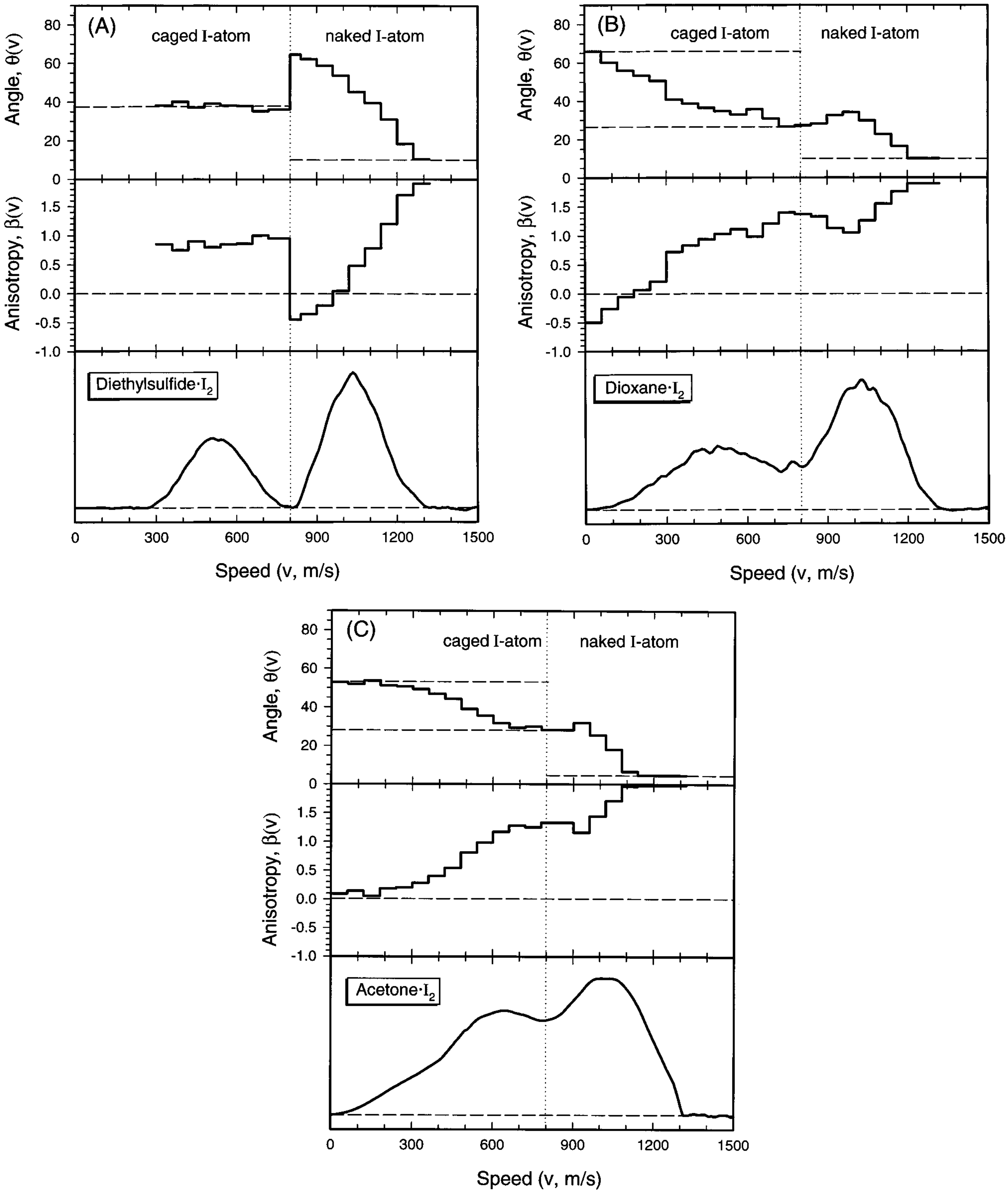

Figure 12. The final (≥7 ps) I-atom speed distributions, anisotropy distributions and corresponding angles between the recoil direction (the bond orientation) and the initial transition dipole moment $\boldsymbol{\mu}_{\mathrm{CT}}$ for (A) diethyl sulfide•I_2, (B) *p*-dioxane•I_2, and (C) acetone•I_2. Note the different anisotropy distributions for the naked, exterior (fast) and caged, interior (slow) I-atoms for each system. The initial angles of the naked, exterior I-atoms and the angle changes of the caged, interior I-atoms are marked by the dashed lines; see the text for detail.

(recoil velocity v) and the initial transition dipole moment ($\boldsymbol{\mu}_{\mathrm{CT}}$). The final recoil anisotropy distributions $\beta(\mathbf{v})$ and the corresponding angles are shown in Figure 12 from a satisfied fitting of both the parallel and perpendicular polarizations of KETOF distributions (at $\chi = 0°$ and 90°) according to eq 8, described in section IIIC, using the derived speed distributions (Figure 9). Figure 13 shows the typical results of the fits for the three complexes at $\chi = 0°$.

For a given value of β, the derived angle could be two values, θ or $180° - \theta$, depending on the relative recoil directions of the two I-atoms. Note that the angle between the recoil velocity of the exterior I-atom and $\boldsymbol{\mu}_{\mathrm{CT}}$ is always less than 90° (θ). However, the recoil direction of the interior I-atom relative to $\boldsymbol{\mu}_{\mathrm{CT}}$ could be either θ or $180° - \theta$ depending on the interior I-atom recoil direction relative to the exterior one. After RET, if most available energy is stored in the I−I bond (potential

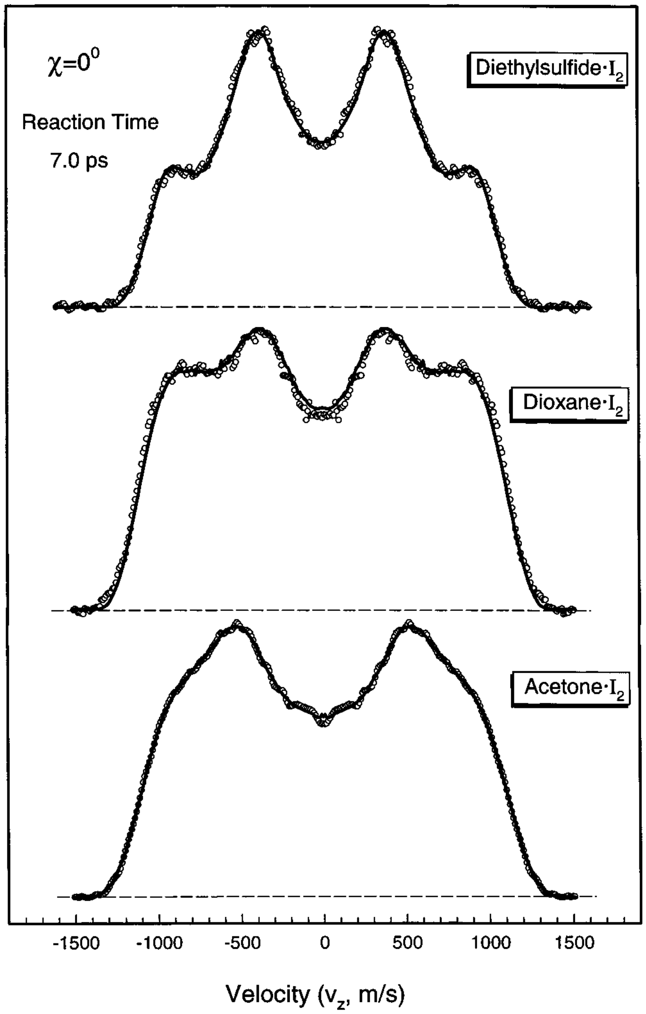

Figure 13. Typical results of the nonlinear least-squares fit of the parallel polarization KETOF distributions for three systems. The open circles are the experimental data and the solid lines are the results of the theoretical simulation. The simulation procedure[29] only uses the first half ($\mathbf{v}_z \leq 0$) of the KETOF distribution; because of symmetry, the second half ($\mathbf{v}_z \geq 0$) of the data here is the replica of the first half.

energy), the interior I-atom will move away from the exterior one and the angle derived from the anisotropy should be 180° $- \theta$ (larger than 90°), and if the D$-$I bond acquires most available energy (translational), the two I-atoms will move the same side away from the donor by three-body dissociation and the corresponding angle should be θ (less than 90°).

The observed fastest exterior I-atoms ($\mathbf{v} \sim 1250-1300$ m/s and $\mathbf{E}_\mathrm{T} \sim 8360-9040$ cm^{-1}) indicate that most available energy is deposited in the I$-$I bond after RET, according to the energy conservation, and there are no other significant vibrations to alter the structure on this initial femtosecond time. Therefore, it is reasonable to consider the complex structure, which releases the fastest exterior I-atoms, as the initial one. From the measured β's of the fastest exterior I-atom release we obtain the angles of the I$-$I bond orientation (recoil velocity) relative to $\boldsymbol{\mu}_\mathrm{CT}$ in the range of 0°-10° (Figure 12) for all three systems.

As discussed in section II, the overall transition dipole moment $\boldsymbol{\mu}_\mathrm{CT}$ in the strong nσ-complex is dominated by the CT-state dipole moment $\boldsymbol{\mu}_{11}$ and the direction points from the donor atoms (S, O) to the center-of-mass of the iodine molecule. Thus, the corresponding angles derived from the β distributions are the relative direction of $\boldsymbol{\mu}_{11}$ and the recoil speed v_I. The observed initial angles, 0°$-$10°, of the fastest exterior I-atoms indicate a nearly linear configuration of S(O)$-$I$-$I for all three complexes, consistent with recent ab initio predictions for the ground-state structures (Figure 4).[55,56] This linear orientation is a perfect geometry for the maximum overlap between the donating orbital (lone-pair electron, p-type) and the accepting orbital σ*. The experimental structures of the three complexes are depicted in Figure 14 and are based on the ab initio predicted interaction scheme.

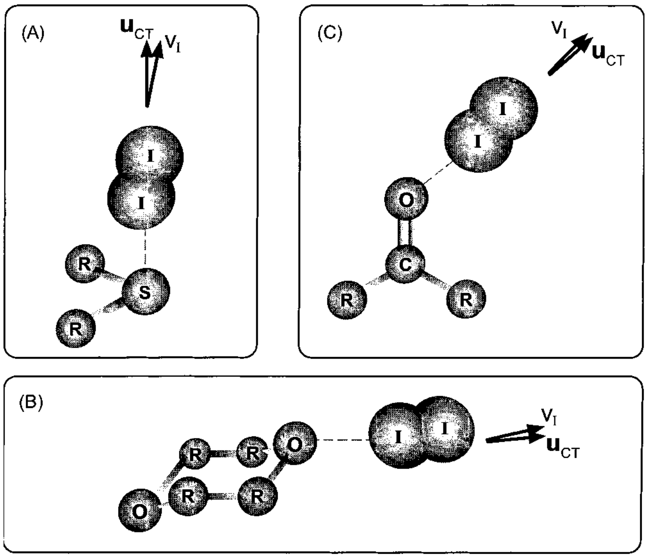

Figure 14. The 1:1 donor$-$acceptor complex structures based on the derived angles between $\boldsymbol{\mu}_\mathrm{CT} \equiv \mathbf{u}_\mathrm{CT}$ and the initial recoil direction $\mathbf{v}_\mathrm{I}$ (and recent ab initio calculations): (A) diethyl sulfide·I$_2$ (R = CH$_3$-CH$_2$), $\theta_{\mathrm{S-I-I}} = 165°$, (B) *p*-dioxane·I$_2$ (R=CH$_2$), $\theta_{\mathrm{O-I-I}} = 172.5°$ and (C) acetone·I$_2$ (R=CH$_3$), $\theta_{\mathrm{O-I-I}} = 165°$. Both directions of $\boldsymbol{\mu}_\mathrm{CT}$ and the initial $\mathbf{v}_\mathrm{I}$ are shown by arrows.

The $\beta(\mathbf{v})$ distributions of the fast exterior I-atoms for the three systems have the similar trend, monotonically decreasing from the same higher value ($\sim$1.9) to a lower one. This observation indicates the structural changes with the energy release. For each system, the two components, naked exterior, and caged interior I-atoms, have different anisotropy distributions. Specifically, for diethyl sulfide·I$_2$ (Figure 12a), the anisotropy β for the fast component monotonically decreases from 1.9 to -0.5 with decreasing the speed and has an average value of $\sim$0.48 and the corresponding angle is 45°, i.e., 35° difference away from the $\boldsymbol{\mu}_\mathrm{CT}$ direction, compared with the initial one. However, the slow I-atoms have a higher, nearly *constant* β's$\sim$0.9, indicating that all interior I-atoms are released nearly along the same direction. For *p*-dioxane·I$_2$ (Figure 12b), the β distribution shows a monotonic decrease from 1.9 to -0.5. The average β for the fast I-atoms is $\sim$1.25 and the corresponding angle is 30°. The slow I-atoms have an average β of $\sim$1.0. For acetone·I$_2$ (Figure 12c), the β distribution for the fast component monotonically decreases, 1.95 to 1.25, with an average of 1.7 and the corresponding angle of $\sim$18°. The slow I-atoms show a monotonic decreasing anisotropy, from 1.25 to 0, and have an average of $\sim$1.0. These correlations of the structural evolution with the energy release for each CT complex will be discussed in more detail in section V.

D. Benzene·ICl: A Direct Examination of Structure and Mechanism. The CT reactions of the 1:1 weak $\pi\sigma$-complexes of benzene (and its deuterated and methyl-substituted species) with I$_2$ have been previously studied in a great detail.[14] The results are similar to those observed for the three nσ-complexes presented in the above. Basically, two speed distributions, fast and slow, were observed and the fast one is from the exterior

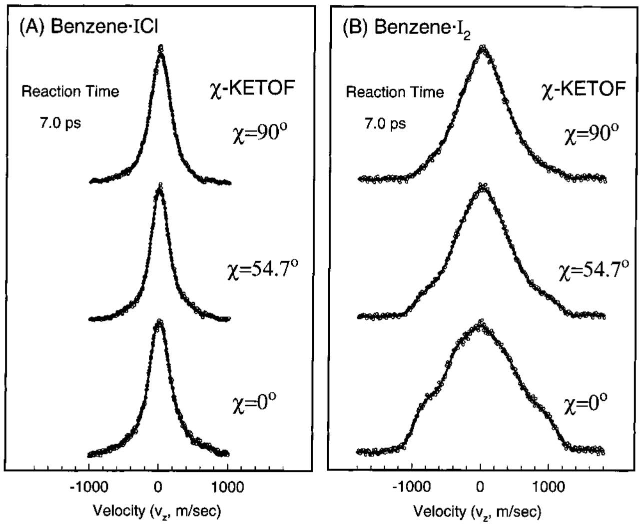

Figure 15. (A) Angular-resolved KETOF distributions of I-atoms for the three different χ's at a fixed delay time of 7.0 ps for benzene•ICl. (B) The results from the benzene•I_2 complex are also shown for comparison.[14] Note that the three velocity distributions of (A) are very similar, narrower and sharper.

I-atoms, released from the dissociative covalent channel, and the slow one is liberated mainly from the one-molecule caging of the interior I-atoms after RET. The contribution of the ionic exit channel to the slow component is minor. The recoil anisotropy for the fast exterior I-atoms was about ~1.0 and the corresponding angle is 35°, indicating that the recoil direction is tilted away from the initial transition dipole, which is also supported by recent ab initio calculations[58] (Figure 4). For the slow interior I-atoms, the anisotropy shows a monotonic decreasing value from 0.6 to 0.1.

The study of the benzene•ICl complex is unique, compared with the benzene•I_2 complex. Using ICl as the electron acceptor instead of I_2, only one I-atom is observed and, therefore, only one speed distribution is expected. If the I-atom faces the benzene molecule in the complex, no I-atoms will be observed from the *ionic* channel on the femtosecond time scale because the Bz^+I^- ion pair (exciplex) usually has a ns lifetime, as many rare-gas halide exciplexes have.[76] But for the dissociative *covalent* pathway after RET, a slow speed distribution will be expected with a reaction time of ~1 ps. If the Cl-atom faces the benzene ring, the exterior I-atom will be released from the *ionic* exit channel with a slow speed distribution, but for the *covalent* channel a fast distribution is expected; the reaction time will be subpicosecond (covalent) to a 1 ps (ionic). Recent ab initio calculations[57] predict a C_s-symmetry structure, similar to the benzene•I_2 one,[58] with the I-atom facing the benzene ring (Figure 4). Thus, only the slow speed distribution of interior I-atoms is expected and on the femtosecond time scale it must be from the dissociative covalent channel, not the ionic one. In the following, the results from both reactions of benzene with ICl and I_2 are presented together for comparison.

The angular-resolved KETOF distributions for three pump polarizations are shown in Figure 15 at a delay time of 7 ps. After 7ps, the distributions stay unchanged and the CT reaction is complete. The three I-atom KETOF distributions from the benzene•ICl complex are surprisingly similar, indicating that the overall anisotropy is very small, close to 0. The much narrower distribution is due to the less total available energy (the strong I−Cl bond) and the dissociation kinematics of ICl, in which the Cl-atom takes more translational energy away. The background I-atom transient KETOF distribution, 15% of the total signal resulting from the ICl molecules alone in the molecular beam, has been subtracted out. The ICl molecule at 277 nm has a pure parallel transition and dissociates into I*+Cl/Cl*,[77,78] and the I-atom KETOF distributions[78,79] ($\beta \sim 2.0$) is totally different from those shown in Figure 15, especially at $\chi = 0°$ and 54.7°.

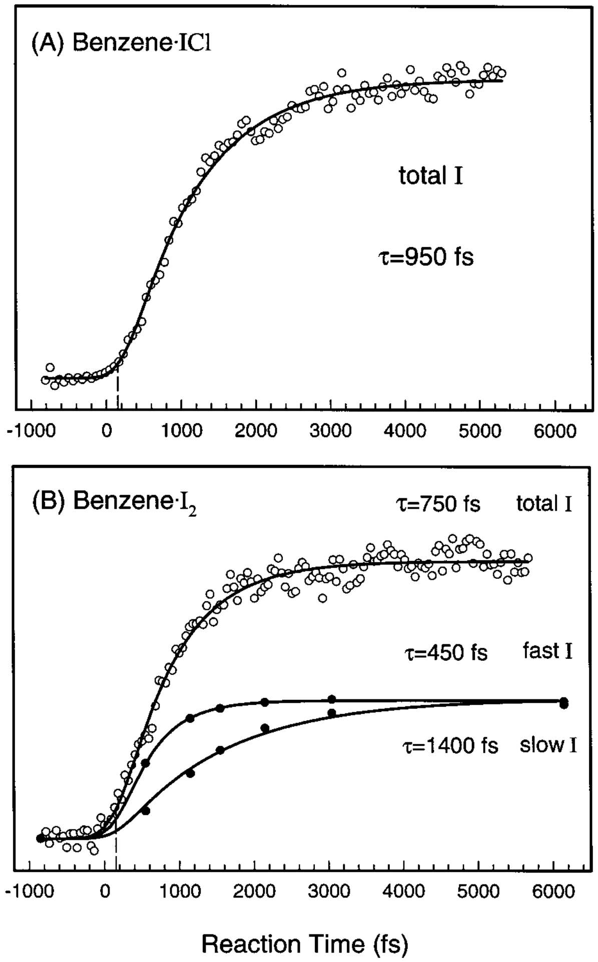

Figure 16. Total iodine atom transients (open circle) and the gated transients (solid circle) of the fast and slow components. Note that only one temporal evolution of I-atoms was observed for benzene•ICl (A). All transients have a ~150 femtosecond coherent shift from the time zero. The branching ratio of the slow to the fast is ~100:100 for benzene•I_2 (B). The solid lines are the theoretical results using a coherent delay (~150 femtosecond) and an exponential rise describing the time evolution (see text).

Comparing the two distributions at $\chi = 0°$ in Figure 15, the fast distribution from the benzene•ICl complex is dramatically reduced and the slow one dominates. The whole distribution shows no significant time dependence, indicating that *all I-atoms are from one dynamic process.* By gating the total I-atoms, the femtosecond transient is shown in Figure 16A with a 950 femtosecond rise time by a single-exponential fit. The KETOF distribution from the benzene•I_2 complex shows two components, fast and slow, with different time behavior (not shown). The fast I-atoms have a 450 femtosecond rise time and the slow ones with 1.4 ps (Figure 16B). The branching ratio of the slow I-atoms to the fast ones is ~100:100, implying that a small percentage of the slow I-atoms is from the exterior ones of the ionic exit channel because there are some trapped interior I-atoms from the covalent channel. All transients have a ~150 femtosecond coherent delay from time zero, similar to that observed in the three nσ-complexes, indicating the coherent nature of the CT reactions and that some trajectories after CT

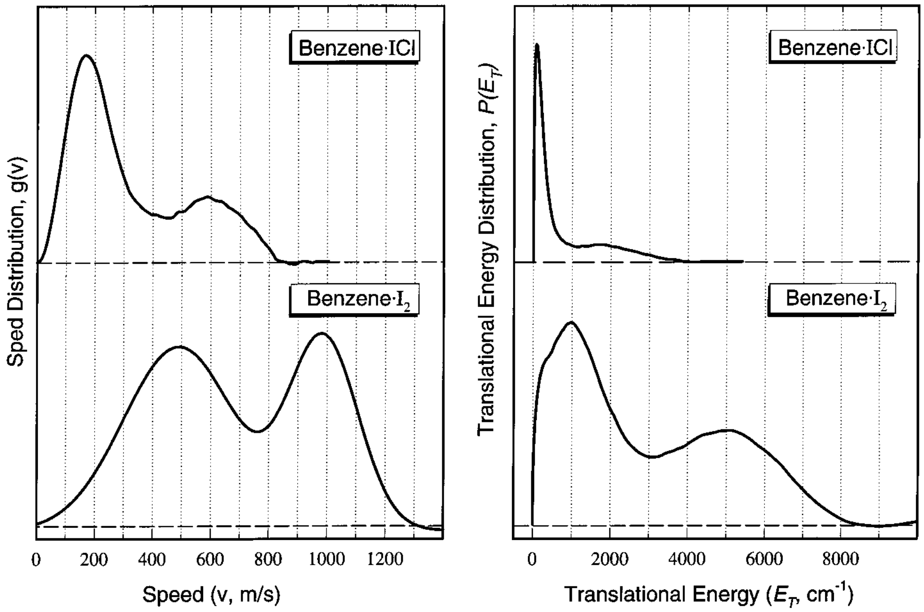

Figure 17. The speed distributions derived from the magic-angle ($\chi = 54.7°$) data shown in Figure 15, together with the corresponding translational energy distributions for (A) benzene•ICl and (B) benzene•I_2. Note the dramatic difference in the high translational energy distributions of both cases.

excitation promptly hop into the covalent channel by RET. The 150 femtosecond coherent shift is simply the bond breaking time of I−Cl on a repulsive potential energy surface.

The final speed distributions derived from the magic angle data (Figure 15) are shown in Figure 17, together with the corresponding translational energy distributions. The whole speed and translational energy distributions for the benzene•ICl complex shifts to the low values as expected. The distribution consists of a major peak centered at **v** ~ 170 m/s and a tail peaking at **v** ~ 585 m/s and extending to ~830 m/s. The major peak accounts for ~75% of the total signal and the tail for 25%. This tail distribution is only from the covalent channel because the ionic channel, even though the Cl-atom faces the benzene ring, could not produce this high-speed I-atom according to the following energetics. The maximum CT absorption is at ~282 nm,[49] and the complex binding energy is assumed to be −3.2 kcal/mol with a distance of 3.0 Å between benzene and Cl.[57] For a complete ET, the Bz^+Cl^- equilibrium distance is derived to be 3.26 Å. To account for a fraction ET, a range of 2.7−3.26 Å is used and the predicted low limit of the zero-point energy of Bz^+Cl^- is ~1.92 eV above its ground state. Therefore, the upper limit of the available energy for the ionic channel is ~0.27 eV at 277 nm excitation and the maximum translational energy of the released I-atom, based on the kinematics, is ~1025 cm^{-1}, much smaller than our observed ~3700 cm^{-1} for the high-speed component. Excluding the high-speed I-atoms from the ionic channel, the slow ones therefore are also from the covalent channel based on two key observations: (1) the high- and low-speed I-atoms show no dramatic temporal difference, thus all I-atoms are released from one dynamical process of the covalent exit channel (shown above); and (2) the anisotropy measurement, discussed next, shows no dramatic difference for the whole I-atoms, indicating that all I-atoms are from the same channel.

The anisotropy distributions by fitting both the parallel and perpendicular KETOF profiles are given in Figure 18, together with the corresponding angles. The typical theoretical simulation of the KETOF distributions is shown in Figure 19 for $\chi = 0°$. The anisotropy distributions show a monotonic decrease from 0.5 to 0 and have the similar values of the caged interior I-atoms from the benzene•I_2 complex (Figure 18), implying that both structures are nearly the same and consistent with the ab initio predictions (Figure 4).[57,58] This observation indicates that *the I-atom faces the benzene ring in the complex structure and all interior I-atoms result from the one-molecule caging of the covalent channel through RET.*

Finally, the two distributions, the major peak and small tail, result from the parallel reaction pathways involving the two spin−orbit states of I* and I (7605 cm^{-1} separation) in the dissociation of ICl. The tail component is centered at ~1830 cm^{-1} and the major peak at ~155 cm^{-1}. The energy difference is ~1675 cm^{-1} and this value is the same *translational* energy separation of I and I* from the dissociation of ICl ($E_{I^*} = m_{Cl}/m_{ICl}E_{avl}$, $E_I = m_{Cl}/m_{ICl}(E_{avl} + 7605) = E_{I^*} + 1673$ cm^{-1}). This observation is very surprising in that, during the inelastic collision between I/I* and benzene, the amount of the transferred atomic translational energy to the benzene moiety is the same for both I and I*. Assuming that the total available energy is deposited in the I−Cl bond after RET, the I-atom acquires 3955 cm^{-1} of translational energy and the I*-atom gets 2329 cm^{-1}. The amount of the energy loss from both I and I* is ~2150 cm^{-1}, an upper limit of the energy transferred to the benzene molecule (C−C motion and molecular rotation) during the collision. The electronic energy of I* was found to be conserved during the collision.[15]

The observed branching ratio of I* to I is 3:1. This ratio represents a lower limit because most trapped iodine atoms are from the I* pathway, which has less available energy and produces slow-speed I*-atoms. Because of the different nature of the potential energy curves of ICl and I_2, this value (3:1) cannot be used to correct the branching ratios of the interior I-atoms to the exterior ones obtained from the D•I_2 reactions (section IVB). Also, because of the less translational energy partition in the I* pathway, more iodine-atoms in the benzene•ICl reaction would be trapped when compared with the D•I_2 reactions. Actually, as discussed in the next section (Sec.VA), the percentage of the caged interior iodine atoms from the I pathway (I+I), hidden in the fast speed distribution of the D•I_2 reactions, is negligible.

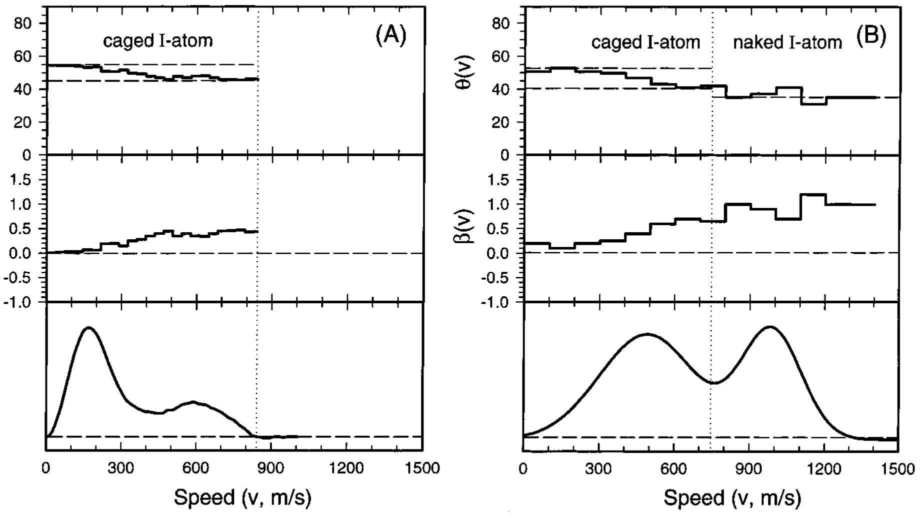

Figure 18. The final (≥7 ps) I-atom speed distributions, anisotropy distributions and corresponding angles between the recoil direction (the bond orientation) and the initial transition dipole moment $\boldsymbol{\mu}_{CT}$. (A) benzene•ICl: Only caged interior I-atoms were detected because the I-atom faces the benzene ring in the complex structure. The anisotropy monotonically decreases from 0.5 to 0. (B) benzene•I_2: The anisotropy for all I-atoms shows a monotonic decreasing from the initial 1.0 to the final 0. The initial angle is about 35°, and the angle changes of the caged interior I-atoms are marked by the dashed lines. Note the similarity of the anisotropy distributions of the caged interior I-atoms for both cases, reflecting the similar complex structures and caging dynamics.

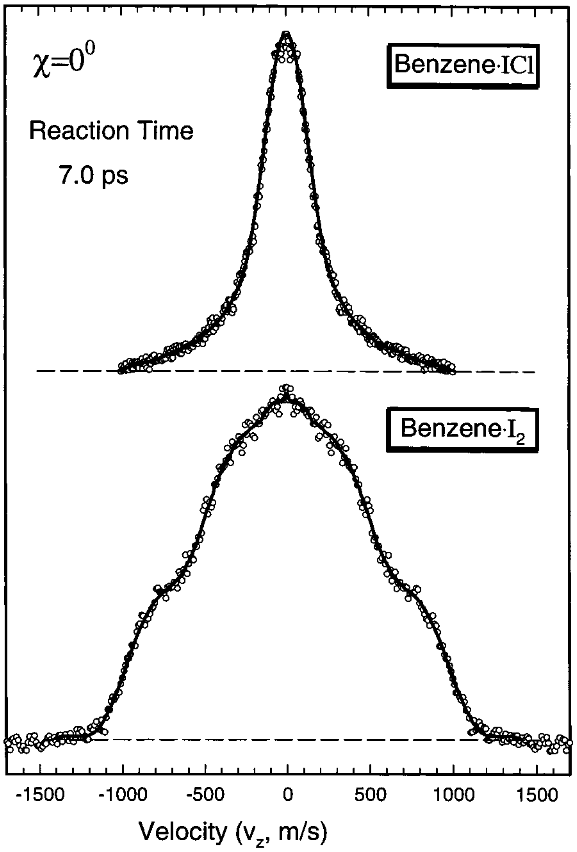

Figure 19. Typical results of the nonlinear least-squares fit of the parallel polarization KETOF distributions for (A) benzene•ICl and (B) benzene•I_2. The open circles are the experimental data and the solid lines are the results of the theoretical simulation. The simulation procedure[29] only uses the first half ($\mathbf{v}_z \le 0$) of the KETOF distribution; because of symmetry, the second half ($\mathbf{v}_z \ge 0$) of the data here is the replica of the first half. Note the dramatic difference in the shapes of the two complexes.

V. Discussion

The experimental results presented above elucidate the mechanism and highlight the concepts of nonconcertedness, caging and restricted energy dissipation in reversible, dissociative ET reactions. The nature of the transition-state dative structure, which is mostly ionic, is important to the vectorial correlation of reaction times, velocities, and orientations (Figure 20, also see Figure 1). The two distinct translational energy distributions of the I-atom product, high and low, result from the two elementary processes involved in the covalent exit channel: The high translational energy distribution of the exterior I-atoms (I_e) reflects the energy dissipation in the dative-bonding TS of the supramolecular $D^+{-}^-I{\cdot\cdot}I^\ddagger$ complex before RET and the low one of the interior I-atoms (I_i) indicates the energy transfer to the donor after the ensuing one-molecule caging (D••I collision) following RET. Thus, the reaction mechanism can be described by the following elementary steps:

$$\begin{array}{lllll} \text{transition state} & & \text{TS} & & \text{products} \\ D^+{-}^-I{\cdot\cdot}I^{*\ddagger} & \rightarrow & D{\cdot}I{\cdot\cdot}I^{*\ddagger} & \rightarrow & D{\cdot}I_i + I_e \\ \text{dative } (\sim\text{ionic}) & & \text{covalent} & & \text{exterior-atom release} \end{array} \qquad (12a)$$

$$\begin{array}{lll} D{\cdot\cdot}I_i{\cdots}I_e & \rightarrow & D + I_i + I_e \\ \text{collision complex} & & \text{interior-atom release} \end{array} \qquad (12b)$$

Reaction 12a indicates a “two-body” (D•I_i and I_e) bond breakage with some interior I-atoms being trapped in the force field of the donor during the inelastic collision. Reaction 12b is an atom−molecule collision process after RET, resulting in a “three-body” (D••I_i•••I_e) decomposition. These two processes are illustrated in Figure 21D, without details of crossings, and in Figure 21A−C with the actual surface crossings. The temporal behavior of the I_e-atom gives the dative-bonding dynamics in the TS before RET. The time evolution of the I_i-atom reflects the entire dynamical process of reaction trajectories from $t = 0$ to the final three-body formation of $D+I_i+I_e$, including the one-molecule caging by nonconcerted and asynchronous concerted pathways (see Figure 21D).

In the following, we discuss the two distinct processes of the dative-bonding TS, and the one-molecule caging after RET.

A. Dative-bonding Transition States. At time zero, the complex in the ground state is promoted in femtoseconds to the dative bonding state, mostly ionic in character, and launching

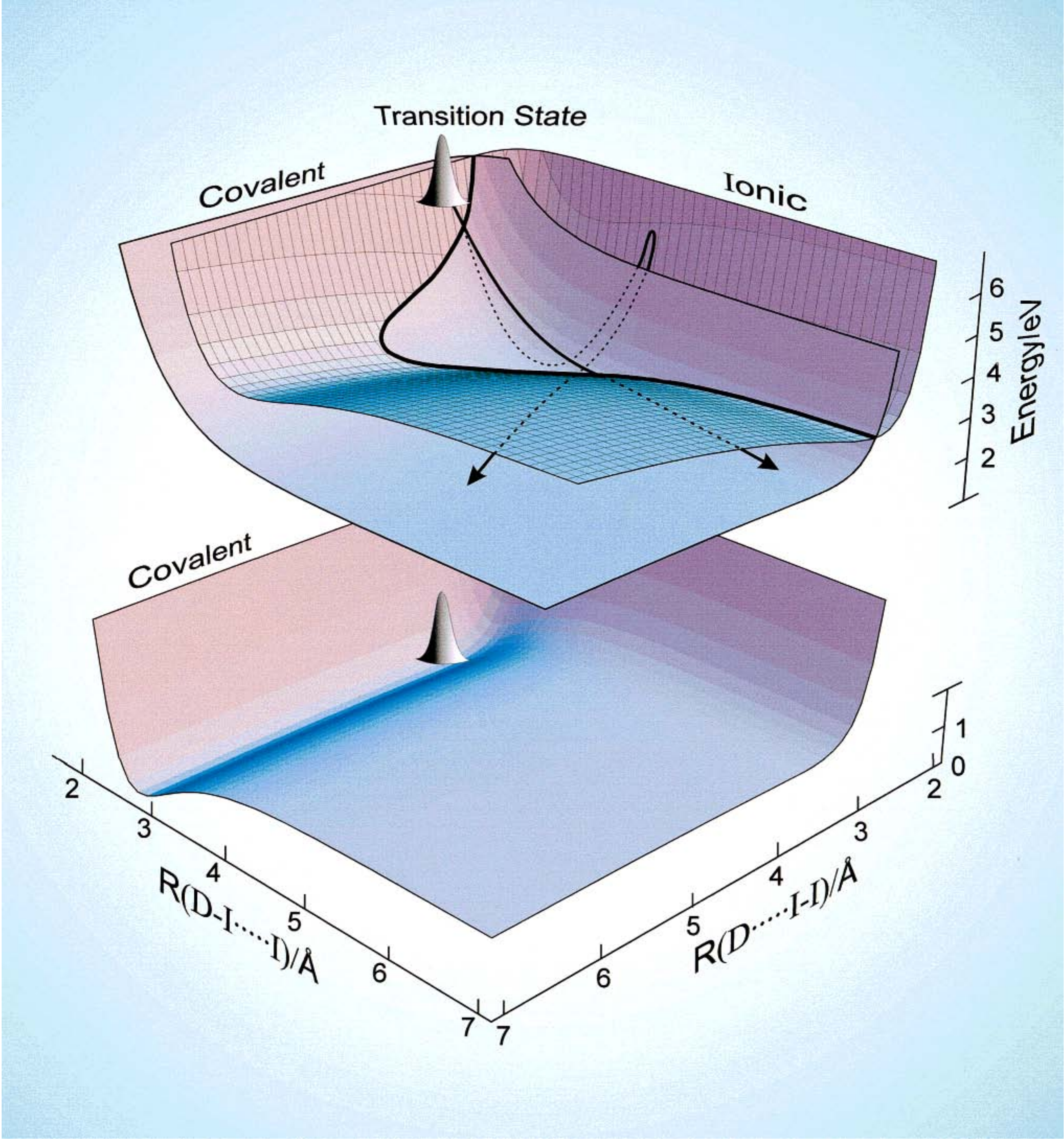

Figure 20. The three-dimensional PESs of the bimolecular complex, calculated for the two reactive coordinates, D···I and I···I, for the neutral ground state, the first CT state and one of the excited dissociative covalent states (I_2* in the C state). The CT PES is drawn for a fraction ET of 89%, which is determined by characteristic of the CT band; this fraction, which reflects the net Coulomb interaction, determines the equilibrium position of the well, see the text. The seam, the crossing of the ionic and covalent PESs, is shown by the thick solid line. Two trajectories, the result of the bifurcation from the first crossing, represent two typical dissociation routes by RET in the dative-bonding TS: One is from the crossing at the smaller r(I−I) and the other results from the electron hopping at the larger r(I−I).

a well-localized nonequilibrium configuration. The initial energy is stored mainly in $D^+{-}I_2^-$ and $I{-}I^-$ bonds and begins the dissipation into other vibrational modes. Figure 20 represents three simplified ground-state, ionic, and covalent PESs, constructed on the two reactive D···I and I···I coordinates, and Figure 21 is the contour maps of the ionic and covalent PESs with a typical trajectory obtained from MD simulations. The prepared wave packet moves toward the dative-bonding TS region after $t = 0$ and the entire complex begins the nuclear motion to search for the new stable structure or the exit channels (Figures 1, 20, and 21). At our excitation energy (36100 cm^{-1}), two exit channels, ionic and covalent, are mainly considered. The ionic channel finishes with $D^+I^-{+}I$ and the covalent channel ends up with two pathways: D•I_2* and D*•I_2. For the covalent channel, RET must occur from the acceptor to the donor.

After the vertical femtosecond excitation at $t = 0$, the I−I bond is weakened (σ*) and the I_2 anion is produced in high vibrational levels, around the dissociation limit.[47] For the ionic channel to release the exterior I-atom, as studied by MD simulations,[14] it takes several picoseconds because of the nature of the attraction in both $D^+{-}I^-$ and $I{-}I^-$ bonds, indicating that

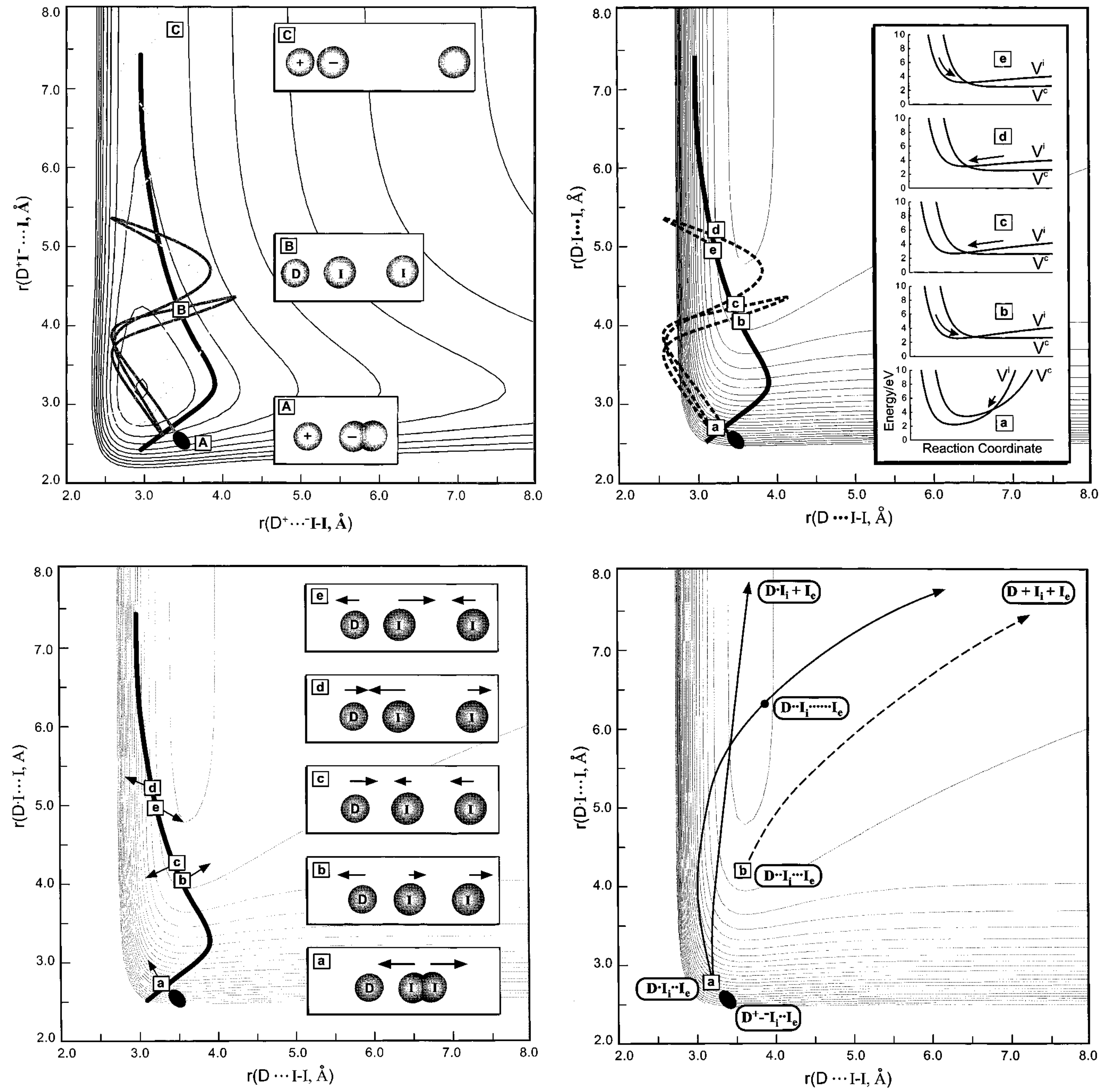

Figure 21. (upper left, A) The energy contour map of the ionic PES of Figure 20. The crossing seam (thick solid line) of the ionic and covalent PESs is also shown. A typical ionic trajectory (dashed line) takes more than 1 ps to reach a distance of 8 Å for $r(\mathrm{I{-}I^-})$. The reactive trajectory (gray solid line) finally evolves along the covalent potential with the multiple crossings in the dative-bonding TS region and this route is the dominant pathway of the CT reactions. Also shown are three snapshots of the structure, assuming a linear configuration, at $t = 0$ (initial wave packet, solid oval), at the seam and in the final ionic product channel if possible. (upper right, B) The energy contour map of the covalent PES of Figure 20 with the crossing seam (thick solid line) and a reactive trajectory (dashed line) in the dative-bonding TS. The potential energy curves (ionic and covalent) cut along the reaction pathway at five, typical, crossing points, one (a) with the smaller $r(\mathrm{I{-}I})$ and the other four (b−e) with the larger $r(\mathrm{I{-}I})$, are shown on the right side. (lower left, C) The energy contour map of the covalent PES of Figure 20 with the crossing seam (thick solid line) and the subsequent moving directions after RET at the five crossings. The corresponding relative motions of D−I and I−I are shown in the five panels on the right. (lower right, D) Illustration of the two processes indicated in eqs 12a and b. Nonconcerted and asynchronous concerted trajectories are schematically shown. They evolve from the two different crossing regions (small $r(\mathrm{I{-}I})$ and large $r(\mathrm{I{-}I})$) and lead to the two-body and three-body reaction channels on the covalent PES.

the entire complex is initially trapped in the dative-bonding region. However, in the dative-bonding TS, an electron from the filled orbital of I_2^- can jump back to the HOMO orbital of the donor to form $D{\cdot}I_2^*$, leaving I_2 still with one electron in the σ^* orbital (repulsive excited states) and releasing the exterior I-atom in ∼150 femtosecond.[29] Clearly, this process is much faster than the ionic one to liberate the exterior I-atom as long as the initial dative-bonding structure takes less than picoseconds to encounter the covalent configuration. The electron involved in the back transfer is different from the initial one because such back transfer will lead to the ground-state $D{\cdot}I_2$, but for the isolated system the energy must be conserved. Thus this transfer, which leaves I_2 in the ground state, will not lead to bond breakage. A σ^*-type configuration, obtained by the CT, requires the jump of another electron.

For the covalent channel of $D^*{\cdot}I_2$, although some probabilities exist for the same initial electron in I_2^- (σ^*) to hop into the excited orbital of the donor,[15] leaving I_2 in the ground state and the donor in the excited state (D*), the chance for this process is minor because of the large change of the I−I configuration and the less overlap of σ^* and the donor excited orbital. Furthermore, the first electronic excited states of diethyl sulfide and *p*-dioxane lie above our excitation energy (36100 cm^{-1}),[63,64] indicating that at least the covalent $D^*\cdot I_2$ channel is not available to these two complexes.

The occurrence of RET in the dative-bonding TS to form $D\cdot I_2^*$ depends on the overlap between one filled orbital of I_2^- and the unpaired HOMO orbital of D and the wave function overlap (Franck−Condon factor) between I_2^- and I_2^*. Thus, the I_2^* states are likely the same states accessed by the optical excitation. Near our excitation energy of 36100 cm^{-1}, there is *only one* optically accessible $C^3\Sigma_{1u}^+$ state, which correlates to I+I*.[68] The electronic configuration of the ground-state I_2^- is $\sigma_g^2\pi_u^4\pi_g^4\sigma_u^1$ (2441) and the C state belongs to $\sigma_g^1\pi_u^4\pi_g^4\sigma_u^1$ (1441). Since the σ_g and σ_u orbitals of I_2 have the same symmetry in the entire complex and can interact similarly with the HOMO orbital of the donor, one electron from the σ_g orbital promptly returns back to the donor (charge recombination) during RET.

There are some optically forbidden, repulsive excited states with the vertical energies close to our excitation energy but the probability to form these states through RET is minor. Specifically, the $^1\Sigma_g^+$ and $^1\Delta_g$ states of the (2422) configuration, which correlate to I*+I* and I*+I, respectively, involve two-electron transfer to two different moieties, one π_g electron to the donor and the other π_g electron to the σ_u orbital. These states are highly unfavored. The other optically forbidden repulsive states are three $^1\Pi_g$, $^3\Pi_{0^+_g}$ and $^3\Pi_{0^-_g}$ states from the (2341) configuration, which all correlate to I*+I, and one $^3\Sigma^+_{0^-_u}$ state of the (1441) configuration which correlates to I+I. RET involves one electron transfer of I_2^- (π_u or σ_g) to the donor. Even though there is a small probability to form these states after RET, most states correlate with a product asymptote yielding I*+I, the same as that of the optically allowed $C^3\Sigma_{1u}^+$ state. Thus, no I_i-atoms are produced from the I pathway (I+I) after RET, as also evidenced from the following energy analysis of the I_e-atom. This conclusion indicates that no I_i-atom distribution is located at the high-speed region under the I_e-atom distribution, as mentioned in section IVD.

From the translational energy distribution of the I_e-atom the CT reaction does evolve *only* along the I* pathway after RET. The distribution reaches the speed limit of the I+I* pathway as determined by the total available energy; see Figure 22. However, the average translation energy of the I_e-atoms is about 5670 cm^{-1} (~1030 m/s), lower than the expected value estimated from the total available energy and indicating that some energy is channeled into the donor "substrate" before RET. Assuming that the I-atoms corresponding to the average translational energy result from the two-body dissociation ($D\cdot I_i+I_e$), the average total translational energy of the entire complex after RET is in the range of 8990−11340 cm^{-1} for diethyl sulfide$\cdot I_2$, 9020−11340 cm^{-1} for *p*-dioxane$\cdot I_2$, and 9560−11340 cm^{-1} for acetone$\cdot I_2$ with two extreme conditions, strong interaction between D and I or no interaction between them, during the I−I dissociation. For the first extreme, we assume that the dissociation first produces an I-atom and a D•I complex and then the complex subsequently falls apart without significant translational energy change, whereas for the second extreme we assume that D is simply a spectator and there is no interaction between D and I. Thus, the expected amount of energy dissipated into the internal modes of the donor substrate before RET is 4680−7030 cm^{-1} for diethyl sulfide$\cdot I_2$, 4680−7000 cm^{-1} for *p*-dioxane$\cdot I_2$, and 4680−6460 cm^{-1} for acetone$\cdot I_2$.

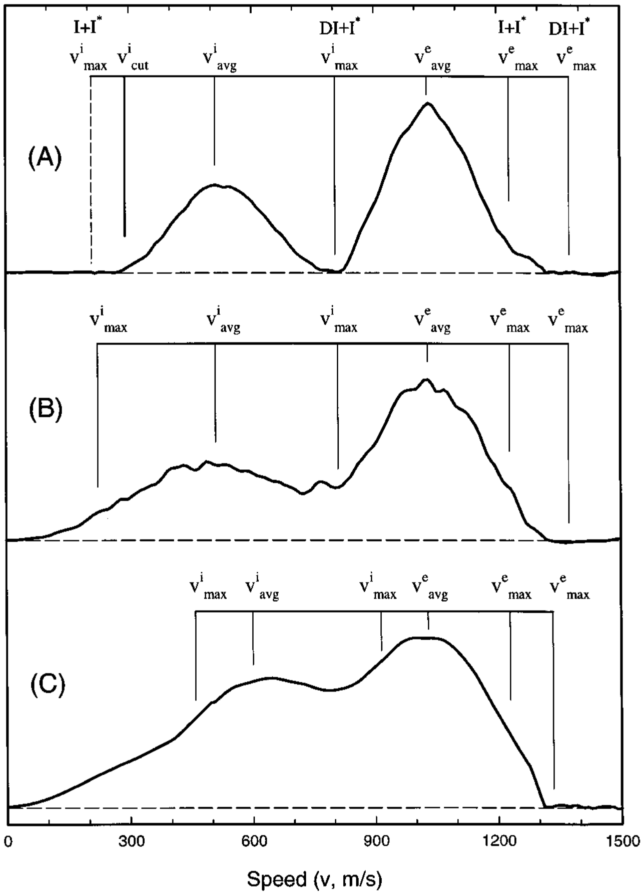

Figure 22. The final (≥7 ps) speed distributions of the three complexes: (A) diethyl sulfide$\cdot I_2$, (B) *p*-dioxane$\cdot I_2$ and (C) acetone$\cdot I_2$. The maximum speeds from the two extreme conditions (see the text) for the exterior and interior I-atoms are shown. Also marked are the average speeds for the both I-atoms of the three complexes and the cutoff speed of the interior I-atom from diethyl sulfide$\cdot I_2$.

If considering the three-body dissociation ($D\cdot\cdot I_i\cdot\cdot\cdot I_e$), the derived internal energy from the extreme condition of strong interaction between D and I is an upper limit for the donor because the three-body dissociation requires more translational energy to produce the I_e-atoms with 5670 cm^{-1} translational energy. The total energy stored in the first CT excitation state is our excitation energy, 36100 cm^{-1}. Therefore, the percentage of the energy flow into the donor before RET is 13%−19.5% for diethyl sulfide$\cdot I_2$, 13%−19.4% for dioxane$\cdot I_2$, and 13%−17.9% for acetone$\cdot I_2$. We conclude that an upper limit of about 19% of the total excitation energy, ~6860 cm^{-1}, is channeled into the donor substrate before RET. Thus, in the dative-bonding TS, the chemical reaction competes with the energy dissipation to the donor substrate and the time scales of RET and the energy redistribution are critical in determining the final outcome of the CT reaction. Probably, there is a small portion of CT reaction trajectories trapped in the TS well (Figure 21) because the energy in the reactive coordinates ($D^+{-}I^-$ and $I{-}I^-$) after the energy dissipation becomes lower than the required energy for forming $D\cdot I_2^*$. This energy-transfer process is very similar to those found in many studies of surface and surface-aligned photochemical reactions.[80−82]

The time scale of the RET process was evidenced in the detection of the I_e-atoms and is less than 1 ps for all systems reported here (Figure 11). On this ultrafast time scale, there is not enough time to reach complete energy redistribution in the entire complex and the dissipated energy probably activates only several internal coordinates of the donor, such as the C−O or C−S motion. The temporal evolution of the dative-bonding TS is illustrated in Figures 20 and 21. At each crossing point of covalent and ionic PESs, the wave packet bifurcates: One part hops into the covalent exit channel by RET and the other remaining one continues on the dative (mostly ionic) surface and is trapped in the TS well to search for another crossing and RET. Basically, there are two crossing areas: One is in the range of the smaller r(I−I) (case a in Figure 21, B−D) and the other is with the larger r(I−I) and r(D−I) (case b−e in Figure 21, B−D). The r(D−I) for the latter crossing area is larger than its initial distance. The exterior I-atoms at the higher speed come from the crossing with the smaller r(I−I) because most available energy is transferred into the potential energy in the I−I bond after RET. The lower-speed exterior I-atoms are mainly from the crossing area with the larger r(I−I) because some energy is transferred into the translational energy in the D−I bond. With the energy dissipation, there is a high crossing probability at the beginning with the smaller r(I−I) and in the later time with the larger r(I−I) because the potential energy is larger at the smaller r(I−I). Our observed broad energy distribution of the exterior I-atoms (∼7.5 kcal/mol at fwhm) is basically due to the distribution of multiple crossings (Figure 21) and the energy dissipation. The fate of each trajectory to evolve to two- or three-body dissociation depends on how much translational energy is stored in the D−I bond during RET and the nature of the interaction between the interior I-atom and the donor, which is discussed in section VB.

The covalent PES of D•I_2* is the same for all CT systems and most ionic PESs have also similar shapes; the difference is only in the constant energy due to the difference in ionization potential (I_D) of the donor; see eq 4. Although the crossing configurations are different for each CT complex, the time for the wave packet to be in the dative-bonding (TS) well would not be dramatically different as long as the total energy in the reactive coordinates before RET is higher than that at the crossing positions. However, this time depends highly on the initial configuration of r(D−I) and the shape of the ionic PES (driving force, similar for most complexes). Experimentally, we observed the survival times of 450, 510, 860, and 830 femtosecond for $Bz^+-{}^-I{\cdot\cdot}I^‡$,[14] $DS^+-{}^-I{\cdot\cdot}I^‡$, $DO^+-{}^-I{\cdot\cdot}I^‡$, $AO^+-{}^-I{\cdot\cdot}I^‡$, respectively. Note that for the two oxygen-containing complexes, the initial configuration of r(O−I) is nearly the same, ∼2.8 Å,[55,56] thus the same lifetimes for the dative-bonding TS, ∼850 femtosecond. The initial configuration of r(S−I) for diethyl sulfide•I_2 is 3.27 Å and that of r(Bz-I) is 3.2 Å for bezene•I_2; thus, the observed similar lifetime is ∼500 femtosecond. MD simulations do indicate that the lifetime of the dative-bonding TS is sensitive to the initial configuration of r(D−I).[14] It should be noted that although the lifetimes are different the dissipated energies into the donor are similar due to the similar accepted modes of the C−O and C−S motions. The slight difference of some higher translational energy distribution of the exterior I-atoms from the acetone•I_2 complex, compared with the other two nσ-complexes, is probably due to the stiff bond of C=O.

For the $\pi\sigma$-benzene•ICl complex, the electronic configuration of ICl is similar to that of the I_2 molecule, but the four states near our excitation energy are all optically allowed transitions and three ones can be accessible during RET process. The other one, ${}^1\Sigma^+_{0+}$ state of the (2422) configuration, is highly unfavored because of the involvement of two-electron transfer. The one ${}^1\Pi_1$ state, correlating to I+Cl*, and other two ${}^3\Pi_{0^+}$ and ${}^3\Pi_1$ states, which correlate to I+Cl, are all from the (2341) configuration and involve one electron transfer from the π_u orbital to the donor HOMO orbital. However, the largest absorption to the ${}^3\Pi_{0^+}$ state at our excitation energy strongly couples to the ${}^3\Sigma^-_{0+}$ state of the (2422) configuration, which correlates to I*+Cl. Thus, both I and I* pathways are involved after RET, as observed in Figure 17, unlike the I_2 case in which only the I* pathway is formed. The formation of the I* pathway in the CT benzene•ICl reaction implies that in the RET process one π_u electron of ICl^- transfers into the donor HOMO orbital and during the ICl dissociation, two π_g electrons of ICl in the (2341) configuration move into its π_u and σ_u orbitals, respectively, to form I*+Cl as asymptotic products from the (2422) configuration.

The vertical electron attachment to ICl at $t = 0$ produces the ICl anion above the dissociation limit. Thus, the dynamics in the dative-bonding TS are different from the Bz•I_2 case because of the nature of the repulsion in the anion I−Cl bond. The TS lifetime of $Bz^+-{}^-I{\cdot\cdot}Cl^‡$ is expected to be much shorter than that obtained for $Bz^+-{}^-I{\cdot\cdot}I^‡$, 450 femtosecond, and the branching ratio of the ionic channel (Bz^+I^-+Cl) should increase. The observed I_i-atoms indicate that the coupling to the covalent channel is so prompt and efficient in such a short time.

The observed ∼150 femtosecond coherent delay time of the fast exterior I-atoms for all systems reported here indicates that the reaction trajectories are coherent. This robust observation originates from the initial well-defined localized wave packet preparation. The observed time is simply the direct bond-breaking time of I_2 on the repulsive surface. Thus, some trajectories after the CT excitation promptly hop into the covalent channel through RET and all available energy is channeled into the I−I bond (potential energy) before any energy dissipation to the donor substrate, as depicted in Figures 20−22. Meanwhile, from the anisotropy of the fastest I_e-atom (∼1250−1300 m/s), we deduced the structure as the initial ground-state one, as shown in Figure 14.

For the fast exterior I-atoms of the three nσ-complexes a strong correlation is observed between β and $\mathbf{v}$ (Figure 12): the lower the speed, the smaller the anisotropy and the larger the corresponding angle, i.e., the less translational energy the exterior I-atom is released with, the larger angle it is tilted away from μ_{CT}. This dynamic correlation with the molecular structure is elucidated from the following three facts. First, after the wave packet experiences the first crossing (smaller r(I−I) in Figs.20 and 21) and moves into the dative-bonding TS, RET occurs at the larger r(I−I) and r(D−I). For a given total energy in the reactive coordinates (D^+-I^- and $I-I^-$), if more translational energy is deposited in the D−I bond and less energy in the I−I bond, the D−I bond stretches longer and the exterior I-atom acquires less translational energy with a lower speed. The longer the D−I bond distance extends, the larger the angle of the I−I bond orientation is altered away from μ_{CT}. This correlation is illustrated in Figure 23.

Second, with the energy dissipation to the donor, the C−S(O) motion of the donor is probably activated and the stretching of the C−S(O) bond makes the I−I bond orientation tilt away from μ_{CT}. The more the energy flows into the C−S(O) motion, the larger the angle of the I−I orientation. Consequently, the exterior I-atom is released with less translational energy and a larger tilted angle after RET. Finally, the anisotropy distributions of the exterior I-atoms for three complexes show a robust monotonic decrease from 1.9 to a lower value, indicating that a bending motion of S(O)−I−I is probably involved after the

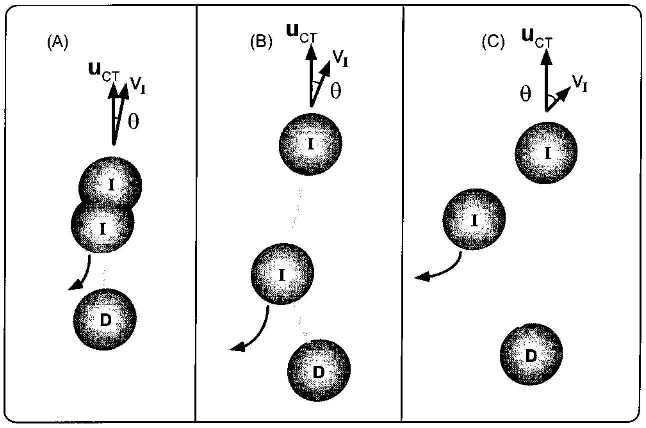

Figure 23. The correlation of the dynamics and the structural evolution is illustrated by the measurement of the exterior I-atom recoil speed and its direction relative to the initial femtosecond alignment, $\boldsymbol{\mu}_{CT} \equiv \mathbf{u}_{CT}$. (A) RET occurs at the smaller r(I−I) and all available energy is deposited in the I−I bond (potential energy), resulting in the largest speed ($\mathbf{v}_I$) with the smallest tilted angle. (B) and (C) RET occurs at the larger r(I−I) with most available energy transformed into the translational energy in both D−I and I−I bonds. In case (B), more translation energy in the I−I bond results in the larger speed with the smaller tilted angle, whereas in case (C) more translational energy in the D−I bond results in the smaller speed with the larger tilted angle. Note that the interior I-atom is moving away from μ_{CT} more than the exterior I-atom by the collision with the donor (D).

initial CT excitation. This observation is especially clear for the diethyl sulfide•I_2 complex and the I−I bond orientation changes from 10° to 60°, relative to μ_{CT}, in the dative-bonding TS. Thus, with the bending-angle increase and more energy dissipation to the donor, the released exterior I-atom after RET has a larger tilted angle with a lower speed.

B. One-Molecule Caging. In the crossing area with the smaller r(I−I), the total energy is mainly deposited in the I−I bond (Figure 21) after RET and the ensuing dynamics of the entire complex can be understood on the basis of the isolated I_2* dissociation and subsequent one-molecule caging. After the direct I−I bond rupture and the release of the I_e-atom, the caged I_i-atom recoils away from the I_e-atom (180° − θ), as shown in Figure 21A. The initial incident angles of the I_i-atom can be obtained from the recoil direction of the I_e-atom. The (remaining) dynamical process is an atom-molecule collision (one-molecule caging) and is determined by the relative collision energy between D and I, the impact parameter, and the binding energy of the D•I complex.

If assuming that all I_e-atoms are from this crossing area, the initial incident angles of the I_i-atoms are ∼170°−120° (relative to μ_{CT}), 170°−150°, and 175°−150° and the initial distributions of the collision energies are 4.1−10.7 kcal/mol (average ∼ 6.7 kcal/mol), 4.0−10.6 kcal/mol (6.6 kcal/mol), and 8.1−3.1 kcal/mol (5.1 kcal/mol) for diethyl sulfide, *p*-dioxane and acetone, respectively. The binding energies of the D•I complexes have been shown in general to be similar to their corresponding molecular I_2 complexes[83] thus they are 6.2 kcal/mol, ∼4.0 and 5.1 kcal/mol for DS•I, DO•I and AO•I, respectively.[55,56] The equilibrium distance between S(O) and I in D•I is slightly larger than that in D•I_2,[58] but the orientation of the I_i-atom to the donor could be very different from that in the D•I_2 complex. Clearly, the D••I complexes are launched at a repulsive, anisotropic PES between D and I in both azimuthal and radial directions. Based on the collision energies and the binding energies, some D•I complexes are trapped in the potential well and never escape.

In the crossing area with the larger r(I−I), the molecular configuration is complicated. In Figure 21, four typical crossings (b−e), assuming a linear configuration, are considered to illustrate the different collision processes between the I_i-atom and the donor after RET. These crossings occur at the larger r(D−I) and r(I−I) than their equilibrium distances. At the 4−5 Å distance of I−I, the repulsive potential energy of the $I_2(C^3\Sigma^+_{1u})$ state is very small and most available energy will transform into the translational energy in both D−I and I−I bonds after RET.

In case b, both D^+-I^- and $I-I^-$ bonds stretch toward the outer turning point and more translational energy is stored in D−I bond after RET. Both I-atoms move in the same direction (θ) and this is a typical three-body dissociation. Case c shows the accelerated attraction interaction in both bonds after reaching the outer turning point and the D−I bond acquires more translational energy after RET. The I_i-atom first collides with the donor, flips the direction and then has a head-on collision with the coming I_e-atom. Both I-atoms exchange the momentum and flip the direction, and the I_i-atom flies away from the I_e-atom, having a corresponding angle of 180°-θ (Figure 12). If the I_i-atom is trapped during the first collision with the donor, the I_e-atom will collide with the D•I complex.

In case d, the D^+-I^- bond has an accelerated attraction interaction and the $I-I^-$ bond stretches toward the outer turning point. The I_i-atom has a head-on collision with the donor, flips the direction with a corresponding angle of θ. Case e is opposite to case (d) and the I_i-atom collides with the I_e-atom, switches the momentum and moves toward the donor with a corresponding angle of 180°-θ (Figure 12). Thus, the recoil direction of the I_i-atom is θ or 180° − θ depending on the relative motion of D−I and I−I during RET. In addition, it should be pointed out that the crossing probability is higher with the smaller r(I−I) and lower with the larger r(I−I) at the beginning, and only when the total energy dissipates into the donor and the total available energy in the reactive coordinates decreases, the crossing at the larger r(I−I) becomes significant. Also, it should be mentioned that although the I_e-atoms, even after RET, are still involved in the one-molecule caging such as in cases c and e, this period of time is very short (∼150 femtosecond) and the observed formation time of the I_e-atom mainly represents the dynamic process in the dative-bonding TS before RET.

Besides the kinematics consideration discussed above, during the collision some available energy can be channeled into the internal modes of D's, reducing the energy available for dissociation of the D•I complex. Although the translation-to-vibration energy transfer (T−V) process is expected to be slow and rather inefficient owing to the weak coupling between the D internal modes and the D−I intermolecular vdW mode, the D−I collision, because of its large binding energy, can result in a collision complex of a new chemical identity. This is the analogue of an intermediate toward chemical reactions and the energy can be transferred to the internal modes of D in a short period of time through a much stronger chemical interaction. This consideration is supported by the results of a cross-beam experiment on Br+chlorotoluene reactions,[84] for which the collision complex was found to have a lifetime shorter than a rotational period (∼5 ps) at collision energies of 20−35 kcal/mol and most available energy is channeled into the internal vibrational modes of the aromatic ring.

For the DS•I complex, we observed that 45% of the I_i-atoms could not be liberated from the force field of DS and the trapped I_i-atom may form a new "chemical" species with DS, such as an inner-sphere CT supramolecule.[85] The anisotropy distribution (Figure 12A) of the escaped I_i-atoms is very striking with a nearly constant value (0.85), indicating that the I_i-atoms are "bound" to DS for certain time and then are released along the same direction. The observed ~800 femtosecond coherent delay time reflects this trapping process and indicates that the fastest trajectories of the escaped I_i-atoms take 800 femtosecond to reach the final $D+I_i$. A similar time behavior was also observed for the $CH_3I{\cdot}I$ collision complex with a 1.4 ps coherent delay time.[86]

The temporal evolution (1150 femtosecond lifetime) of the escaped I_i-atoms integrates the entire dynamic process including the time behavior in the dative-bonding TS and the subsequent one molecule caging after RET. The first dynamical process takes 510 femtosecond (lifetime) from the detection of the I_e-atoms and the entire process needs 1150 femtosecond, indicating that the one-molecule caging finishes in 1−2 ps. From the translational energy distribution of the I_i-atoms, the fraction of the I_i-atom energy transferred in the caging is ~80% (5133 cm^{-1}) and 47% of the transferred energy (2400 cm^{-1}) goes into the internal energy and 53% (2733 cm^{-1}) to the translational energy of diethyl sulfide, assuming the crossing at the smaller $r(I-I)$ during RET. The energy transfer is very efficient in such a short time, supporting the new chemical species involved. This is further supported by the observation of the speed cutoff at 300 m/s, indicating a new chemical species with a dissociation barrier of ~3.7 kcal/mol (upper limit). This inelastic energy transfer is also evident in the temporal shift of the slow speed component with the time in Figures 1A and 9A.

For the two oxygen-containing CT complexes, the anisotropy distributions of the caged I_i-atoms are very similar for both complexes and show a monotonic decrease, indicating that the I_i-atoms are scattered by the donor away from the incident angles (Figure 23), quite different from the DS··I complex. Although the binding energy for the DO·I complex is smaller than that for the AO·I one, the energy transfer must be more efficient because 35% of the I_i-atoms are trapped in DO·I, whereas only 12% in AO·I. The energy distributions of the escaped I_i-atoms support the observed branching ratios. Assuming that RET occurs at the smaller $r(I-I)$, for the DO·I complex the fraction of the I_i-atom energy transferred in the caging is ~78% (4785 cm^{-1}) and 50% of the transferred energy (2393 cm^{-1}) is channeled into the internal modes of *p*-dioxane and the other 50% into its translational energy. This efficient energy-transfer process is very similar to the DS··I complex, but the temporal behavior is different. The escaped I_i-atoms only have a ~150 femtosecond coherent delay, similar to that of the I_e-atoms, indicating no significant trapping time during the caging and the involvement of three-body dissociation such as case b in Figure 21. The dynamics in the dative-bonding TS show a lifetime of 860 femtosecond, and the entire time evolution from the escaped I_i-atoms has a 2.23 ps lifetime. Thus, the caging takes about 2−3 ps.

For the AO··I complex, the fraction of the I_i-atom energy transferred in the caging is ~66% (3748 cm^{-1}) and 56% of the transferred energy (2089 cm^{-1}) is coupled into the internal modes of acetone and the other 44% (1659 cm^{-1}) into its translational energy. Compared with the DO··I complex, less translational energy of the caged I_i-atoms is transferred to acetone, which is probably due to the stronger C═O bond. The temporal evolution of the caging is very similar to that of the DO··I complex (2−3 ps) whereas the entire complex has a lifetime of 830 femtosecond and the whole dynamic process of the escaped I_i-atoms has a 2.1 ps lifetime. Nevertheless, the T−V energy transfer is so efficient in such a short time for these two complexes thus this process must involve some "loose" new chemical species.

For the benzene·ICl weak complex, the entire dynamic process of the escaped I_i-atoms has a 950 femtosecond lifetime, shorter than that for the benzene·I_2 complex (1.4 ps). This observation results from the following: The initial I_i-atoms after RET have much lower translational energy than that of the benzene·I_2 complex and more caged I_i-atoms are expected to be trapped; the process in the dative-bonding TS is much shorter for the benzene·ICl complex because of the nature of repulsion in the $I-Cl^-$ bond, as discussed in section VA. Comparing the weak benzene·I_2 complex with the oxygen-containing complexes, the process for benzene·I_2 (1.4 ps lifetime) is faster than that for *p*-dioxane·I_2 (2.23 ps) and that for acetone·I_2 (2.1 ps) and this is due to the shorter dynamical time scale in the dative-bonding TS (450 femtosecond lifetime), whereas the lifetime of the corresponding process takes 860 femtosecond in *p*-dioxane·I_2 and 830 femtosecond in acetone·I_2. In fact, the caging takes nearly the similar time of 2−3 ps.

VI. Conclusion

The *time, speed,* and *orientation* resolution of dynamics of CT reactions is a powerful approach for dissecting the different elementary processes, elucidating the mechanism and the molecular structure. The CT supramolecular complex evolves along the dissociative covalent channel by reversible ET and the reaction proceeds by two distinct pathways: The primary process in the dative-bonding transition state region involves the dynamically active space of nuclear motions which lead to some energy dissipation to the donor substrate, with the probability of crossing to the covalent surface following RET. This process occurs on the femtosecond time scale and is monitored by the release of the *exterior* I-atom; the first coherent trajectory takes ~ 150 femtosecond. The second dynamical process after RET is the one-molecule caging. This caging takes more than 1 ps to liberate the *interior* I-atom. The energy transfer of the atomic motion to the donor substrate in this process of caging is very efficient and is evident in the clear shift of the speed distributions with time. The efficient trapping on such short time scales and the highly directional ejection from the substrate suggest the formation of a new chemical species during the inelastic collision. The correlation of the dynamics and the structural evolution during the entire process is also elucidated by the measurement of the recoil speed and its direction relative to the initial femtosecond complex alignment.

These studies emphasize several concepts. First, the *reversibility* of ET, which leads to a dominant covalent pathway, is an important mechanism and could be general in the so-called harpoon reaction mechanism. Second, the separation of time scales for the two dynamical processes by RET indicates the *nonconcertedness* between ET and the chemical bond breakage, a point of debate in many areas of studies. Moreover, the appearance of *coherent* reaction trajectories is evidence of the localized nuclear wave packet motion. Third, the dynamics of *energy dissipation* to the donor substrate in the dative-bonding TS critically depends on the time scales of RET and bond breakage. On the ultrashort time scale, this energy dissipation is not dominant. In the cases reported here, an upper limit of ~19% of the *total* excitation energy dissipates as internal energy of the donor substrate. Thus only few internal coordinates can be activated since there is not enough time to reach complete energy redistribution. This concept of dynamically active space should be important in studies of surface and surface-aligned photochemical reactions.[80−82]

The interplay between the structure and the ensuing dynamics is rationalized with the help of LUMO−HOMO interactions

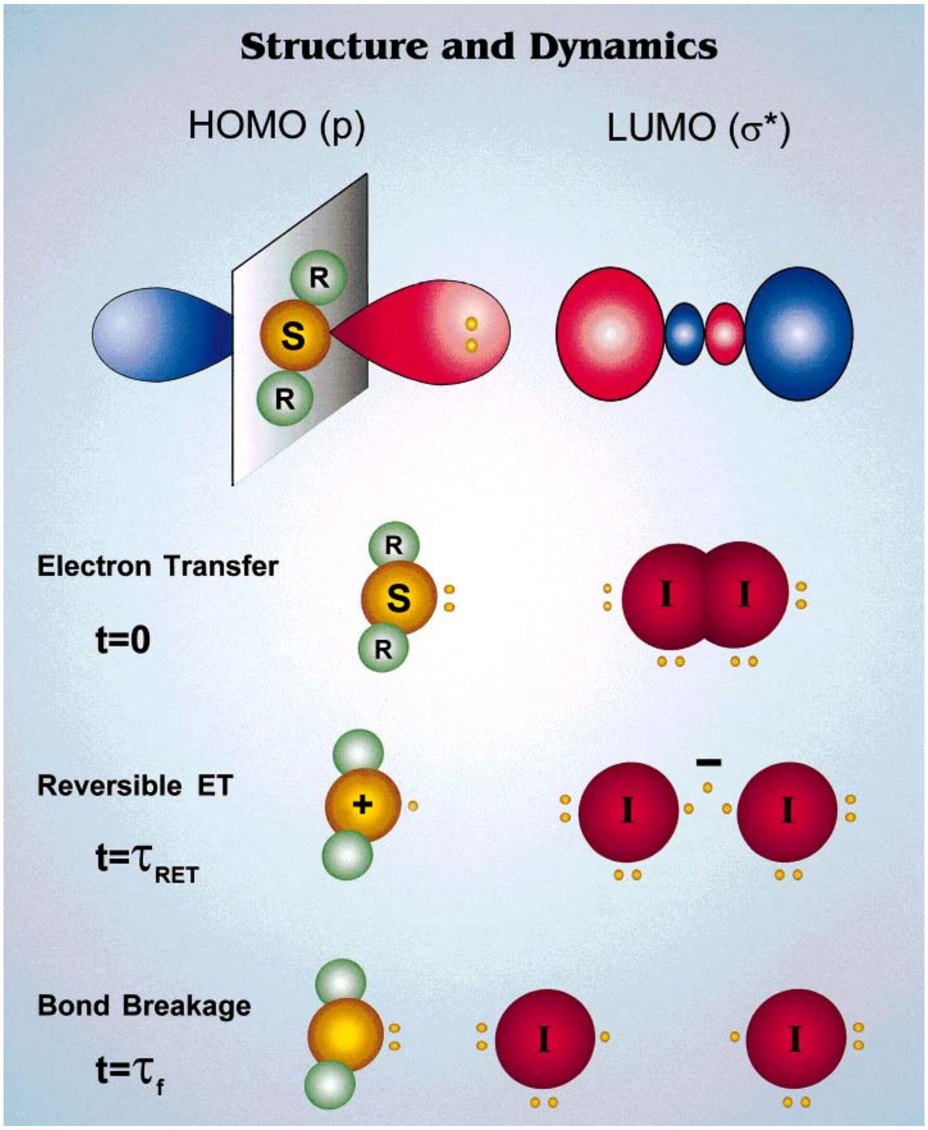

Figure 24. Frontier orbital representation of the concept of RET, and the correlation of dynamics and structure in the reversible and dissociative electron-transfer reactions. Note that two *different* electrons are involved in the reaction as discussed in the text. The ultrafast RET shifts the dominance toward the covalent channel and the I−I bond rupture.

(Figure 24). As depicted in Figures 1, 20, and 21, the initial structure, corresponding to the wave packet at zero time, has mostly ionic character with the transferred electron being in the σ^* LUMO of the I−I bond. When the trajectory of the motion reaches the seam between ionic and covalent PESs and an electron goes back to the donor, the acceptor I_2 (or ICl) system is in an equivalent structure to that of an $n\sigma^*$ repulsive potential (Figure 24). Thus, the reason for the dominance of trajectories on the covalent potential by RET can now be understood. The trapping in the Coulomb potential (ionic channel) takes much longer time than the rupture on the repulsive surface (covalent channel) which releases the exterior I-atom. Hence it is the time scale of the nuclear motion which shifts the dominance toward the covalent bond breakage following RET.

On the ultrashort time scale, the dynamics and mechanism for the isolated reactions should have strong correlation to those in the condensed phase especially in nonpolar solvents. The formation of the D·I complex in solution has two distinct time scales, 25−250 femtosecond and ∼400 femtosecond. Given our picture, we suggest that the species "D·I" in solution is actually the $D{\cdot}I_i$ in our picture; its formation in 25−250 femtosecond reflects the prompt RET in solution and corresponds to the dynamical process of the I_e-atoms (<150−500 femtosecond) in the gas phase. The second process in solution involves the formation of a $D'{\cdot}I_e$ complex and this mimics the one-molecule caging for the trapped I_i-atoms (∼1ps) in the gas phase. Both pathways are somewhat faster in solution because the time for the appearance of the D·I complex in solution is shorter than the time for the I_e- and I_i-atoms to be detected as free fragments from the isolated complex, i.e., in solution the distance traveled is shorter. The random solute−solvent interactions may also enhance the coupling of the ionic and covalent potentials. The formation of ground-state iodine molecules in solution is also understood. As mentioned in the text, the overlap of the σ^* orbital (I_2^-) and the donor excited orbital (D^*) is less favorable for the isolated system. However, in solution this could be enhanced because of structural fluctuations, resulting in I_2 formation from $D^*{\cdot}I_2$. In addition, a fast geminate recombination (I−I) may occur, as observed for I_2 in dense fluids and liquids.[87] Longer-time (10s of ps) processes in solution typically reflect the onset of vibrational relaxation, which we observed clearly in our studies of clusters of I_2 in benzene.[88,58] One final point is that both the isolated reactions and those in liquids share the importance of RET as it would not be possible to detect D·I in solutions if ET persists to form D^+I^-.

Acknowledgment. This work is supported by a grant from the National Science Foundation, the Airforce Office of Scientific Research and the Office of Naval Research. T.M.B., a Feodor Lynen Fellow from the Alexander von Humboldt Foundation, acknowledges the foundation and Caltech for support.

References and Notes

(1) Lewis, G. N. *Valence and the Structure of Atoms and Molecules*; The Chemical Catalog Co.: New York, 1923.

(2) Pauling, L. *The Nature of the Chemical Bond*; Cornell University Press: New York, 1939.

(3) Mulliken, R. S. *J. Am. Chem. Soc.* **1950**, *72*, 610; *J. Am. Chem. Soc.* **1952**, *74*, 811.

(4) Mulliken, R. S.; Person, W. B. *Molecular Complexes: A Lecture and Reprint Volume*; Wiley-Interscience: New York, 1969.

(5) Benesi, H. A.; Hildebrand, J. H. *J. Am. Chem. Soc.* **1949**, *71*, 2703.

(6) Briegleb, G. *Elektronen-Donor−Acceptor-Komplexe*; Springer: Berlin, 1961.

(7) Yarwood, J., Ed.; *Spectroscopy and Structure of Molecular Complexes;* Plenum: New York, 1973.

(8) Foster, R., Ed. *Molecular Complexes;* Elek Science: London, 1973.

(9) Gur'yanova, E. N.; Gol'dshtein, I. P.; Romm, I. P. *Donor−Acceptor Bond*; John Wiley: New York, 1975.

(10) Langhoff, C. A.; Gnädig, K.; Eisenthal, K. B. *Chem. Phys. Lett.* **1980**, *46*, 117.

(11) Hilinski, E. F.; Rentzepis, P. M. *J. Am. Chem. Soc.* **1985**, *107*, 5907.

(12) Lenderink, E.; Duppen, K.; Wiersma, D. A. *Chem. Phys. Lett.* **1993**, *211*, 503. Lenderink, E.; Duppen, K.; Everdij, F. P. X.; Mavri, J.; Torre, R.; Wiersma, D. A. *J. Phys. Chem.* **1996**, *100*, 7822. Everdij, F. P. X.; Wiersma, D. A.; Spoel, D. V.; Mavri, J.. In *Femtochemistry and Femtobiology: Ultrafast Reaction Dynamics at Atomic-scale Resolution*; Sundström, V., Ed.; Imperial College Press: Singapore, 1997.

(13) Pullen, S.; Walker, L. A., II.; Sension, R. J. *J. Chem. Phys.* **1995**, *103*, 7877. Walker, L. A., II.; Pullen, S.; Donovan, B.; Sension, R. J. *Chem. Phys. Lett.* **1995**, *242*, 177.

(14) Cheng, P. Y.; Zhong, D.; Zewail, A. H. *J. Chem. Phys.* **1995**, *103*, 5153; *J. Chem. Phys.* **1996**, *105*, 6216.

(15) DeBoer, G.; Burnett, J. W.; Fujimoto, A.; Young, M. A. *J. Phys. Chem.* **1996**, *100*, 14882. DeBoer, G.; Burnett, J. W.; Young, M. A. *Chem. Phys. Lett.* **1996**, *259*, 368.

(16) Castleman, A. W., Jr.; Bowen, K. H., Jr. *J. Phys. Chem.* **1996**, *100*, 12911. Castleman, A. W., Jr., Ed. *J. Phys. Chem. A* **1998**, *102* (23).

(17) Lineberger, W. C.; Nadal, M.; Nandi, S.; Wenthold, P.; Kim, J. B.; Andersen, L. H.; Ozaki, Y.; Boo, D. W. In *Femtochemistry and Femtobiology: Ultrafast Reaction Dynamics at Atomic-scale Resolution*; Sundström, V., Ed.; Imperial College Press: Singapore, 1997.

(18) Greenblatt, B. J.; Zanni, M. T.; Neumark, D. M. *Science* **1997**, *276*, 1675; *J. Chem. Soc., Faraday Discuss.* **1997**, *108*, 101. Zanni, M. T.; Greenblatt, B. J.; Neumark, D. M. *J. Chem. Phys.* **1998**, *109*, 9648. Lehr, L.; Zanni, M. T.; Frischkorn, C.; Weinkauf, R.; Neumark, D. M. *Science* **1999**, *284*, 635.

(19) Ayotte, P.; Bailey, C. G.; Weddle, G. H.; Johnson, M. A. *J. Phys. Chem. A* **1998**, *102*, 3067. Ayotte, P.; Weddle, G. H.; Kim, J.; Kelley, J.; Johnson, M. A. *J. Phys. Chem. A* **1999**, *103*, 443.

(20) Boivineau, M.; Calvé, J. L.; Castex, M. C.; Jouvet, C. *J. Chem. Phys.* **1986**, *84*, 4712; *Chem. Phys. Lett.* **1986**, *128*, 528; *Chem. Phys. Lett.* **1986**, *130*, 208. Jouvet, C.; Boivineau, M.; Duval, M. C.; Soep, B. *J. Phys. Chem.* **1987**, *91*, 5416.

(21) Nelson, T. O.; Setser, D. W.; Qin, J. *J. Phys. Chem.* **1993**, *97*, 2585. Huang, F.; Setser, D. W.; Cheong, B. S. *Isr. J. Chem.* **1994**, *34*, 127.

(22) Chang, X. Y.; Ehlich, R.; Hudson, A. J.; Polanyi, J. C.; Wang, J.-X. *J. Chem. Phys.* **1997**, *106*, 3988. Topaler, M. S.; Truhlar, D. G.; Chang, X. Y.; Piecuch, P.; Polanyi, J. C. *J. Chem. Phys.* **1998**, *108*, 5378.

(23) Zadoyan, R.; Apkarian, V. A. *Chem. Phys. Lett.* **1993**, *206*, 475. Hill, M. H.; Apkarian, V. A. *J. Chem. Phys.* **1996**, *105*, 4023.

(24) Eberson, L. *Electron-Transfer Reactions in Organic Chemistry*; Springer: Berlin, 1987. Eberson, L. *Acta Chem. Scand.* **1999**. In press.

(25) Savéant, J.-M. *Adv. Phys. Org. Chem.* **1990**, *26*, 1. Robert, M.; Savéant, J.-M. *Photoinduced Dissociative Electron Transfer. Is the Quantum Yield Equal to Unity*; 1999. In press.

(26) Marcus, R. A. *Angew. Chem., Int. Ed. Engl.* **1993**, *32*, 1111.

(27) Fox, M. A., Ed. *Chem. Rev.* **1992**, *92* (3).

(28) Zewail, A. H. *Femtochemistry: Ultrafast Dynamics of the Chemical Bond*; World Scientific: Singapore, 1994.

(29) Zhong, D.; Zewail, A. H. *J. Phys. Chem. A* **1998**, *102*, 4031.

(30) Zhong, D.; Zewail, A. H. *Proc. Natl. Acad. Sci. U.S.A.* **1999**, *96*, 2602.

(31) Andrews, L. J. *Chem. Rev.* **1954**, *54*, 713. McGlynn, S. *Chem. Rev.* **1958**, *58*, 1113.

(32) Andrews, L. A.; Keefer, R. M. *Molecular Complexes in Organic Chemistry*; Holden-Day: San Francisco, 1964.

(33) Rose, J. *Molecular Complexes*; Pergamon Press: Oxford, 1967.

(34) Rao, C. N. R.; Bhat, S. N.; Dwivedi, P. C. *Appl. Spectrosc. Rev.* **1971**, *5*, 1.

(35) Tamres, M.; Goodenow, J. M. *J. Phys. Chem.* **1967**, *71*, 1982; *J. Chem. Phys.* **1965**, *43*, 3393.

(36) Friedrich, H. B.; Person, W. B. *J. Chem. Phys.* **1966**, *44*, 2161.

(37) Ogimachi, N.; Andrews, L. J.; Keefer, R. M. *J. Am. Chem. Soc.* **1955**, *77*, 4202.

(38) Drepaul, I.; Fagundez, V.; Guiterrez, F.; Lau, E. H.; Joens, J. A. *J. Org. Chem.* **1996**, *61*, 3571.

(39) Bhat, S. N.; Rao, C. N. R. *J. Am. Chem. Soc.* **1968**, *90*, 6008.

(40) Koll, M. *J. Am. Chem. Soc.* **1968**, *90*, 1097.

(41) Tamres, M.; Bhat, S. N. *J. Am. Chem. Soc.* **1972**, *94*, 2577.

(42) Garito, A. F.; Wayland, B. B. *J. Phys. Chem.* **1967**, *71*, 4062.

(43) McCullough, J. D.; Zimmermann, I. C. *J. Phys. Chem.* **1961**, *65*, 888.

(44) Bhat, S. N.; Rao, C. N. R. *J. Am. Chem. Soc.* **1966**, *88*, 3216.

(45) Klaboe, P. *J. Am. Chem. Soc.* **1967**, *89*, 3667.

(46) Wobschall, D.; Norton, D. A. *J. Am. Chem. Soc.* **1965**, *87*, 3559.

(47) Chen, E. C. M.; Wentworth, W. E. *J. Phys. Chem.* **1985**, *89*, 4099. Dojahn, J. G.; Chen, E. C. M.; Wentworth, W. E. *J. Phys. Chem.* **1996**, *100*, 9649.

(48) Rao, C. N. R.; Chaturvedi, G. C.; Bhat, S. N. *J. Mol. Spectrosc.* **1970**, *33*, 554.

(49) Andrews, L. J.; Keefer, R. M. *J. Am. Chem. Soc.* **1952**, *74*, 4500. Andrews, L. J.; Keefer, R. M. *J. Am. Chem. Soc.* **1950**, *72*, 5170.

(50) Hubers, M. M.; Kleyn, A. W.; Los, J. *Chem. Phys.* **1976**, *17*, 303. Auerbach, D. J.; Hubers, M. M.; Baede, A. P. M.; Los, J. *Chem. Phys.* **1973**, *2*, 107.

(51) Person, W. B. *J. Chem. Phys.* **1963**, *38*, 109.

(52) Gol'dshtein, I. P.; Kharlamova, E. N.; Gur'yanova, E. N. *Z. O. Khim.* **1968**, *38*, 1984.

(53) Syrkin, Y. K.; Anisimova, K. M. *Dokl. Akad. Nauk.* **1948**, *59*, 1457. Price, A. H.; Brownsell, V. L. In *Molecular Relaxation Processes, Chemical Society Special Publication No. 20*; Academic Press: Washington, DC, 1966.

(54) Fairbrother, F. *J. Chem. Soc.* **1948**, 1051. Bhat, S. N.; Rao, C. N. R. *J. Am. Chem. Soc.* **1968**, *90*, 6008.

(55) Ammal, S. S. C.; Ananthavel, S. P.; Chandrasekhar, J.; Venuvanalingam, P.; Hegde, M. S. *Chem. Phys. Lett.* **1996**, *248*, 153.

(56) Setokuchi, O.; Shimizu, Y. *J. Mol. Struct. (THEOCHEM)* **1993**, *281*, 67.

(57) Ammal, S. S. C.; Ananthavel, S. P.; Venuvanalingam, P.; Hegde, M. S. *J. Phys. Chem. A* **1998**, *102*, 532.

(58) Su, J. T.; Zewail, A. H. *J. Phys. Chem. A* **1998**, *102*, 4082.

(59) Hassel, O. *Acta Chem. Scand.* **1962**, *19*, 2259.

(60) Reiling, S.; Besnard, M.; Bopp, P. A. *J. Phys. Chem. A* **1997**, *101*, 4409.

(61) Hassel, O. *Proc. Chem. Soc.* **1957**, 250. Hassel, O.; Stromme, K. O. *Acta Chem. Scand.* **1958**, *12*, 1146. Hassel, O.; Romming, C.; Tufte, T. *Acta Chem. Scand.* **1961**, *15*, 967.

(62) Lamoreaux, R. H.; Giauque, W. F. *J. Phys. Chem.* **1969**, *73*, 755.

(63) Hearn, C. H.; Turcu, E.; Joens, J. A. *Atmos. Environ.* **1990**, *24A*, 1939. Thompson, S. D.; Carroll, D. G.; Watson, F.; O'Donnell, M.; McGlynn, S. P. *J. Chem. Phys.* **1966**, *45*, 1367.

(64) Hernandez, G. J.; Duncan, A. B. F. *J. Chem. Phys.* **1962**, *36*, 1504. Cornish, T. J.; Baer, T.; Pedersen, L. G. *J. Phys. Chem.* **1989**, *93*, 6064. Moreno, P. O.; Shang, Q. Y.; Bernstein, E. R. *J. Chem. Phys.* **1992**, *97*, 2869.

(65) Calvert, J. G.; Pitts, J. N. *Photochemistry*; John Wiley: New York, 1966. Lee, E. K. C.; Lewis, R. S. *Adv. Photochem.* **1980**, *12*, 1. Baba, M.; Hanazaki, I.; Nagashima, U. *J. Chem. Phys.* **1985**, *82*, 3938.

(66) Tamres, M.; Duerksen, W. K.; Goodenow, J. M. *J. Phys. Chem.* **1968**, *72*, 966. Passchier, A. A.; Gregory, N. W. *J. Phys. Chem.* **1968**, *72*, 2697.

(67) Seery, D. J.; Britton, D. *J. Phys. Chem.* **1964**, *68*, 2263.

(68) Mulliken, R. S. *J. Chem. Phys.* **1971**, *55*, 288.

(69) Clear, R. D.; Wilson, K. R. *J. Mol. Spectrosc.* **1973**, *47*, 39.

(70) Hwang, H. J.; El-Sayed, M. A. *J. Phys. Chem.* **1991**, *95*, 8044.

(71) The dissociation of I_2 at 277 nm leads exclusively to I and I* with an anisotropy close to -1 by the χ-KETOF measurements of I-atoms. Besides, a broad peak, ∼30−40% of the total signal, near zero velocity $\mathbf{v}_z$ with an isotropic distribution ($\beta \sim 0$) was also observed, a slow process attributed to a dissociative autoionization from a long-lived Rydberg state reached by two-photon absorption.[72]

(72) de Vries, M. S.; van Veen, N. J. A.; Baller, T.; de Vries, A. E. *Chem. Phys.* **1981**, *56*, 157.

(73) Tamagake, K.; Kolts, J. H.; Setser, D. W. *J. Chem. Phys.* **1979**, *71*, 1264.

(74) Donovan, R. J.; Greenhill, P.; MaDonald, M. A.; Yencha, A. J.; Hartree, W. S.; Johnson, K.; Jouvet, C.; Kvaran, A.; Simon, J. P. *J. Chem. Soc., Faraday Discuss.* **1987**, *84*, 221.

(75) The binding energy of DS•I is taken to be similar to that of DS•I_2, similar to the results in ref 58. The bonding in DS•I is not pure van der Waals in nature, probably including a mixture of ionic and covalent characters.

(76) Dunning, T. H.; Hay, P. J. *J. Chem. Phys.* **1977**, *66*, 1306. Hakuta, K.; Fujino, M.; Nakayama, K.; Takuma, H. *Jpn. J. Appl. Phys.* **1990**, *29*, 1194. Quinones, E.; Yu, Y. C.; Setser, D. W.; Lo, G. *J. Chem. Phys.* **1990**, *93*, 333.

(77) Ni, C.; Flynn, G. W. *Chem. Phys. Lett.* **1993**, *210*, 333. Tonokura, K.; Matsumi, Y.; Kawasaki, M.; Kim, H. L.; Yabushita, S.; Fujimura, S.; Saito, K. *J. Chem. Phys.* **1993**, *99*, 3461. Rogers, L. J.; Ashfold, M. N. R.; Matsumi, Y.; Kawasaki, M.; Whitaker, B. J. *Chem. Phys. Lett.* **1996**, *258*, 159.

(78) Jung, K. W.; Ahmadi, T. S.; El-Sayed, M. A. *J. Phys. Chem. A* **1997**, *101*, 6563.

(79) The dissociation of ICl at 277 nm leads to a dominant channel of I*+Cl/Cl* ($\geq$90% branching ratio) with an anisotropy close to ~2 and a minor channel of I+Cl/Cl* ($\leq$ 10%) with $\beta \sim -1$, from the χ-KETOF measurements of I-atoms. Similar to the I_2 case,[71] another additional broad peak, ~30−40% of the total intensity near zero $\mathbf{v}_z$ velocity, shows an isotropic distribution ($\beta \sim 0$). This slow process is probably due to a dissociative autoionization of a long-lived Rydberg state, reached by a two-photon absorption.

(80) Garrett, S. J.; Heyd, D. V.; Polanyi, J. C. *J. Chem. Phys.* **1997**, *106*, 7847.

(81) Hellberg, L.; Strömquist, J.; Kasemo, B.; Lundqvist, B. I. *Phys. Rev. Lett.* **1995**, *74*, 4742. Ho, W. *Surf. Sci.* **1994**, *299/300*, 996.

(82) Tripa, C. E.; Yates, J. T. *Nature* **1999**, *398*, 591.

(83) Porter, G.; Smith, J. A. *Proc. R. Soc. London, Ser. A* **1961**, *261*, 28. Strong, R. L. *J. Phys. Chem.* **1962**, *66*, 2433.

(84) Robison, G. N.; Continetti, R. E.; Lee, Y. T. *J. Chem. Phys.* **1988**, *89*, 6226.

(85) Hörmann, A.; Jarzeba, W.; Barbara, P. F. *J. Phys. Chem.* **1995**, *99*, 2006. Jarzeba, W.; Thakur, K.; Hörmann, A.; Barbara, P. F. *J. Phys. Chem.* **1995**, *99*, 2016.

(86) Zhong, D.; Cheng, P. Y.; Zewail, A. H. *J. Chem. Phys.* **1996**, *105*, 7864.

(87) Lienau, C.; Zewail, A. H. *J. Phys. Chem.* **1996**, *100*, 18629; and references therein for all other work.

(88) Cheng, P. Y.; Zhong, D.; Zewail, A. H. *Chem. Phys. Lett.* **1995**, *242*, 369.